Dual hydrocarbon–geothermal energy exploitation: potential synergy between the production of natural gas and warm water from the subsurface

Author for correspondence:
Jeroen van der Molen,
Email: Jeroen.vandermolen@tno.nl

Jeroen van der Molen[1] , Elisabeth Peters[1], Farid Jedari-Eyvazi[2] and Serge F. van Gessel[1]

[1]TNO, Princetonlaan 6, 3584 CB, Utrecht, the Netherlands and [2]GESciTech, 33 Wood Street, Barnet, Hertfordshire EN5 4BE, UK

Abstract

The decline of domestic natural gas production, increasing dependency on gas imports and lagging development of renewable energy production may pose serious challenges to the current high standards of secure energy supply in the Netherlands. This paper examines synergy between hydrocarbon- and geothermal exploitation as a means to reinforce energy security. The Roden gas field is used as an example to demonstrate potential delay of water breakthrough in the gas well and a resulting increase of recovered gas (up to 19%), by positioning of a geothermal doublet in the water leg of the gas field. The reservoir simulations show that the total increase of gas production primarily depends on the amount of aquifer support. An optimal configuration of gas- and geothermal wells is key to maximise gas recovery and strongly depends on the distribution of reservoir properties. The study also reveals that this option can still be beneficial for gas fields in a late stage of production.

Net Present Value calculations show that the added value from the geothermal doublet on total gas production could lead to an early repayment of initial investments in the geothermal project, thereby reducing the overall financial risk. If no subsidies are taken into account, the additional profits can also be used to finance the geothermal project up to break-even level within 15 years. However, this comes with a cost as the additional profits from improved gas recovery are significantly reduced.

Introduction

The energy system in the Netherlands is subject to substantial changes. The Dutch *Energieagenda* (MEA, 2016) targets a 95% reduction of greenhouse gas emissions, compared to the 1990 emissions levels, by 2050. In this respect, the replacement of fossil fuels (coal, gas, oil) by clean and renewable sources (wind, solar, biomass and geothermal) represents one of the key pillars of climate and energy policies. However, as domestic production of natural gas steadily declines, the fossil-to-renewable transition becomes more urgent. The high investment costs associated with a rapid transition, the disappearing backbone of secure fossil energy production and the measures to balance the high shares of intermittent renewables may form a challenging hurdle to this transition. Synergies between natural gas production and development of renewable production may help to mitigate these issues.

The Netherlands has proven to be one of the largest natural gas producers in the European Union (Juez-Larré et al., 2016; Honoré, 2017). Over the past 70 years both the on- and offshore territories have been thoroughly explored and produced (Breunese et al., 2005; Geluk & De Jager, 2012). Natural gas production in the Netherlands has steadily declined since 2014, however, as most fields enter tail-end production while the rate of new discoveries being added to the portfolio is decreasing (MEA, 2018). The impacts of induced earthquakes related to gas production from the Groningen gas field (Van Geuns & Van Thienen-Visser 2017) have led to the decision by the Dutch government to lower the annual production from the Groningen gas field to 12 billion cubic metres (BCM) per annum and to fully halt production by 2030 (Wiebes, 2018). However, a later statement by the Dutch government declares that production from the Groningen gas field could be (close to) 0 from 2022 onwards (Wiebes, 2019). Furthermore, the coalition agreement of the Dutch government states that onshore no new exploration licences for hydrocarbons will be awarded (Rutte et al., 2017). Consequently, the Netherlands is shifting from being a leading natural gas exporter in western Europe to being a net importer of natural gas (Van Geuns et al. 2017), while simultaneously trying to phase out natural gas as an energy source. As the development of renewables in the Netherlands is lagging, the demand for natural gas in the Netherlands remains significant, with more than 50% of electricity
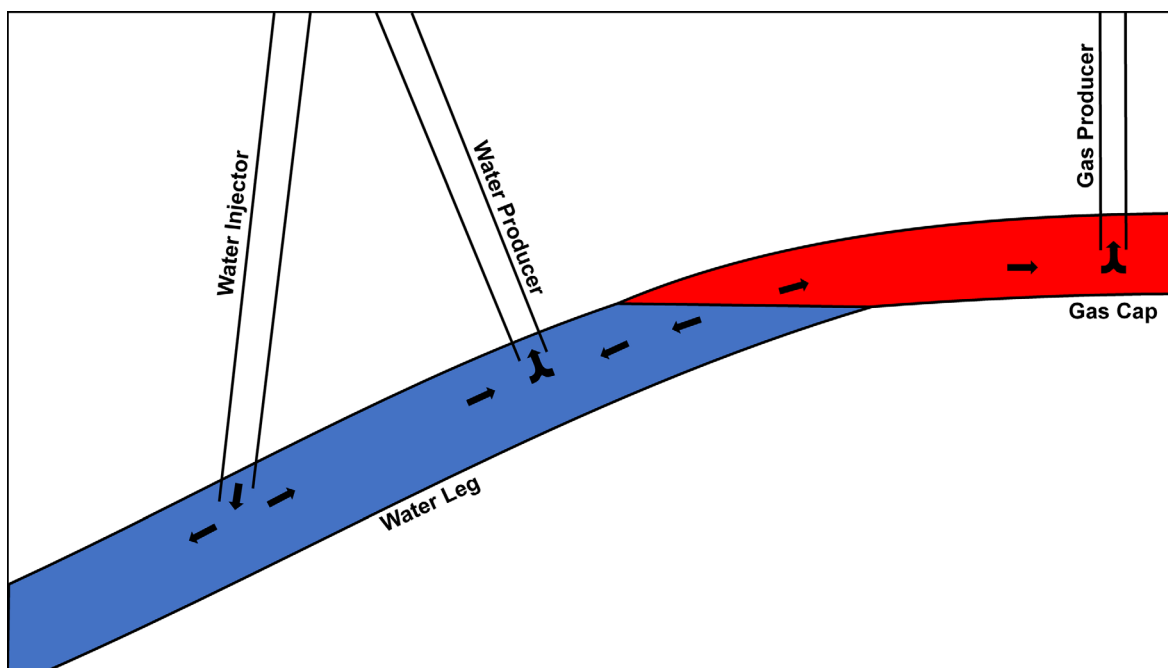
Figure 1. Dual hydrocarbon–geothermal energy exploitation.

being generated by natural gas and 96% of all Dutch households using natural gas as a heating source (Van der Sar, 2014).

Sustainable energy sources like geothermal energy can partially replace natural gas as an energy source for heating demand. In a typical low-enthalpy geothermal system (<150°C; Franco & Vaccaro, 2013) hot water is produced from an aquifer, after which the energy is extracted through a heat exchanger. The cooled water is subsequently reinjected in the same aquifer via a second well (Pluymaekers et al., 2012), thereby forming a geothermal doublet. Over recent decades, numerous studies have investigated the potential for geothermal energy development in the Netherlands (RGD, 1983; Rijkers & Van Doorn, 1997; TNO-NITG, 2004; Kramers et al., 2012). Recent assessments claim that geothermal production may contribute up to 50 petajoules (PJ) of geothermal heat in 2030 and more than 200 PJ in 2050 (DAGO et al., 2018). This would imply that nearly 25% of the expected total heat demand in the Netherlands (870 PJ) would originate from geothermal energy. Since the development of the first geothermal doublet in the Netherlands in 2008, 19 more systems have been realised. As of January 2018 these systems provide 3 PJ of geothermal energy, which is mostly used to heat greenhouses (MEA, 2018). The growth sought by the geothermal sector in the Netherlands is hampered by high investment costs and the long duration and/or risk of return of such investment (Van der Donk, 2008; Veldkamp et al., 2018).

The Dutch Mining Act allows exploration and production licences for hydrocarbons to coexist and overlap with those for geothermal purposes. Additionally, the conventional target reservoirs for hydrocarbons are often identical to those considered for geothermal resources, i.e. sandstone formations of Lower Cretaceous, Upper-Jurassic, Triassic and Permian age. Co-production of dissolved gas and, in rare cases, oil is observed at most of the geothermal systems in the Netherlands (MEA, 2018). The potential interference between geothermal and oil/gas exploration- and production activities within these licences poses a challenge to operators of both types of assets, policy makers and health, safety and environment supervisors. However, this coexistence can also present

synergetic opportunities for both activities. Van Wees et al. (2014) propose a dual play concept for exploration of natural gas and geothermal prospects, aiming for an improvement of the risked-value-to-investment ratio and the expected monetary value of a project. This concept assumes that an exploration well failing to prove the presence of hydrocarbons (dry well) may technically be successful in tapping a hot-water-bearing reservoir. If conversion and completion for geothermal exploitation is anticipated during well design and project planning, the abandonment costs are deferred to a later stage and the investments pay out a geothermal production or injection well. The dual play concept is currently pursued in various locations in the Netherlands (Savelkous, 2018).

A second type of synergy between hydrocarbon and geothermal exploitation may be achieved by converting former hydrocarbon production wells into geothermal wells. This can either be done by reusing a single well and converting it into a Deep Borehole Heat Exchanger (Van Wees et al., 2007; Davis & Michaelides, 2009), or by reusing multiple wells and converting them into a (doublet) system of geothermal producers and injectors (RGD, 1987; Daarnhouwer 2013; Godderij et al., 2018). This concept is being investigated for the depleted Middenmeer gas field where two out of three gas production wells are considered for conversion into geothermal wells (Savelkous, 2016).

A third synergy concept for hydrocarbon and geothermal production is proposed by Aramburo Velez (2017) and Ziabakhsh-Ganji (2018). In this case a geothermal well produces hot water, part of which is utilised in the normal way for residential or greenhouse heating. The other part is sent through a heater and injected into an oil-bearing reservoir where the injected hot water lowers the viscosity of the heavy oil, ultimately increasing the recovery factor (EOR).

This paper presents a fourth concept of synergy, in which a geothermal doublet consisting of one producer and one injector is placed in the water leg of a gas field close to a producing gas well (Figure 1). With the appropriate configuration of producers and injectors, the production of water from the water leg through the geothermal production well slows down water encroachment
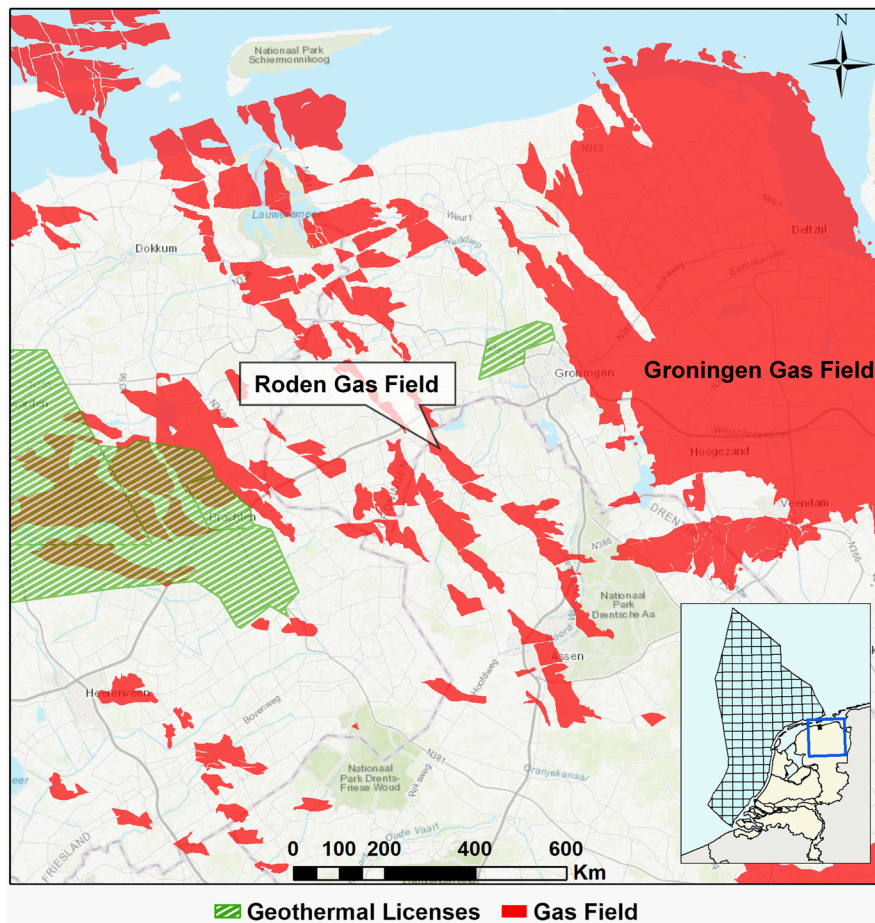
Figure 2. Map of Groningen area and its gas fields, highlighting location of the Roden and Groningen gas fields.

in the gas cap and thus delays the timing of water breakthrough at the gas production well. Consequently the production lifetime of the gas well is extended and the ultimate gas recovery is increased (Peters et al., 2014; Van der Meulen, unpublished MSc thesis, 2016). This paper presents and discusses the results of an in-depth sensitivity analysis based on this concept, using a reservoir model of the Roden gas field as a test case.

The Roden gas field

The Roden gas field is located in the northeastern part of the Netherlands, west of the Groningen gas field (Figure 2). The well ROD-01 (nowadays called ROD-101) discovered the field in 1970. The field consists of two fault blocks with major bounding faults delineating the northern, western and southern field margins, and a gentle eastward slope on the eastern side (Figure 3). In 1976, the well ROD-102 was drilled targeting the centre of the crest in the main fault block. Subsequently, the well ROD-201 (and sidetrack) was drilled targeting the southern block. Following this drill sequence, the field was brought onstream. ROD-201 already ceased production in 1984 due to a high water cut. In 1988, ROD-101 also suffered severe water production, but was sidetracked updip (ROD-101-S2). The remaining wells produced until 2002, when ROD-102 ceased natural gas production following liquid loading. The year after, ROD-101-S2 also stopped producing; all wells are currently (ready to be) abandoned. In total, 6.5 BCM has been produced, resulting in a recovery factor of nearly 70% (NAM, 2003). In its production life, the reservoir pressure has dropped from 345 to roughly 100 bar. However, ten years after

cessation of production, reservoir pressure has increased back to 187 bar (Godderij et al. 2018). While the initial decrease in pressure suggests a depletion drive, the relatively early breakthrough of water and the recovery of reservoir pressure after production ceased also suggests the presence of a moderate aquifer drive.

The reservoir of the Roden gas field comprises the Permian Upper Rotliegend Group. Initial production of natural gas occurred from the Slochteren Sandstone Formation (ROSL). This formation consists mainly of a sequence of good porous and permeable sandstones and conglomerates with minor intercalations of claystone (Van Adrichem Boogaert & Kouwe, 1997). In the study area the ROSL is of fluvial origin (Geluk, 2007). Based on the well log data, the thickness of the ROSL is between 140 and 220 m. The upper 20 to 30 m of the ROSL in the Roden gas field is more shaly in nature. The Ten Boer Member (ROCLT) of the Silverpit Formation conformably overlies the ROSL. This interval of mostly sandy clay- and siltstones also contains numerous sandstone stringers. The ROCLT was deposited in a lacustrine (playa) setting (Geluk, 2007). Thickness of ROCLT in the Roden gas field ranges between 20 and 30 m. In later stages of production, the ROCLT was perforated and produced. The Upper Rotliegend Group is covered by the strata of the Zechstein Group, of which especially the thick sequences of rock salt act as a regional seal (Geluk, 2007).

Methodology and results

In order to test the potential synergy between hydrocarbon- and geothermal energy production at the Roden gas field, a static reservoir model of the main segment of this gas field was created using
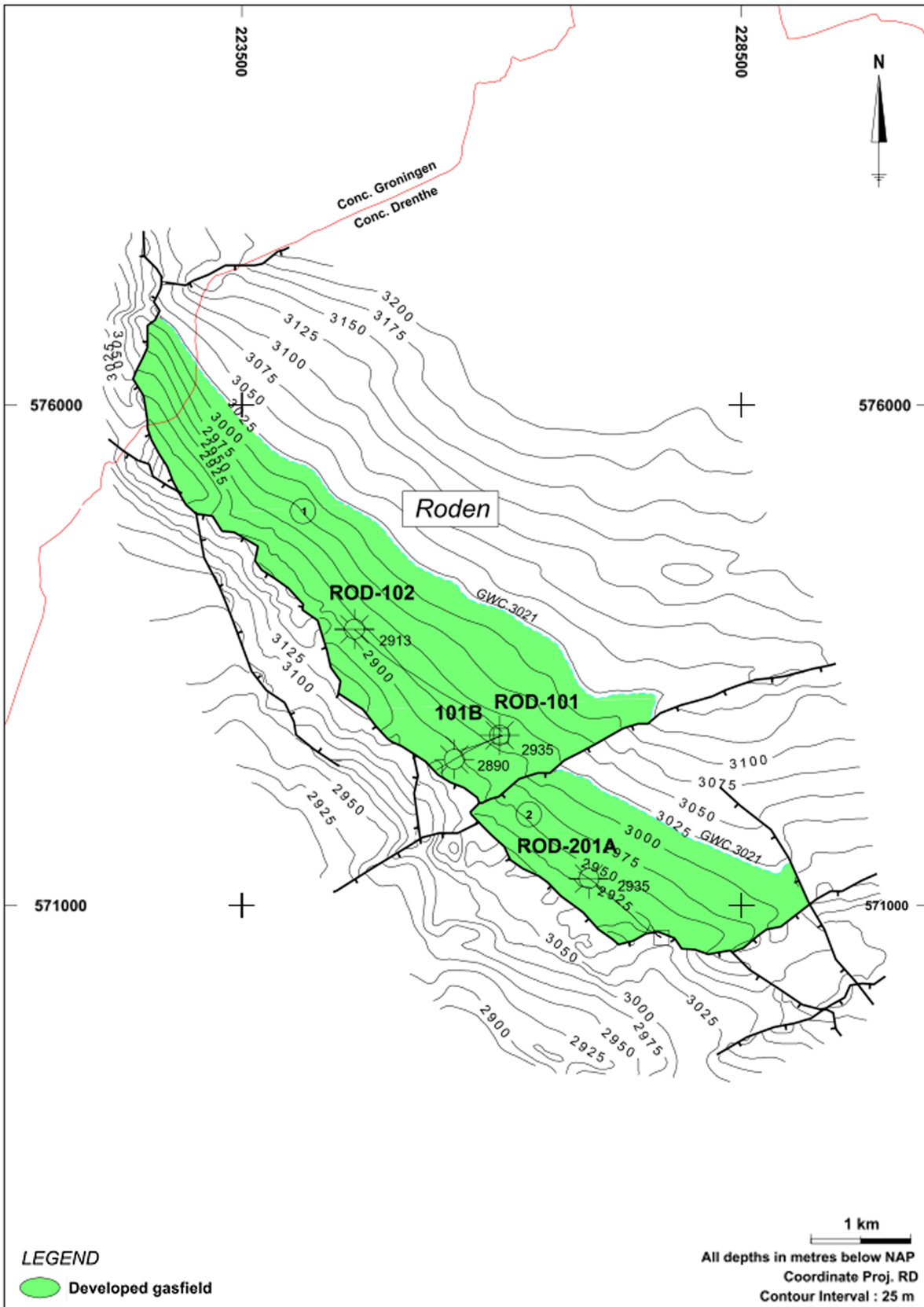
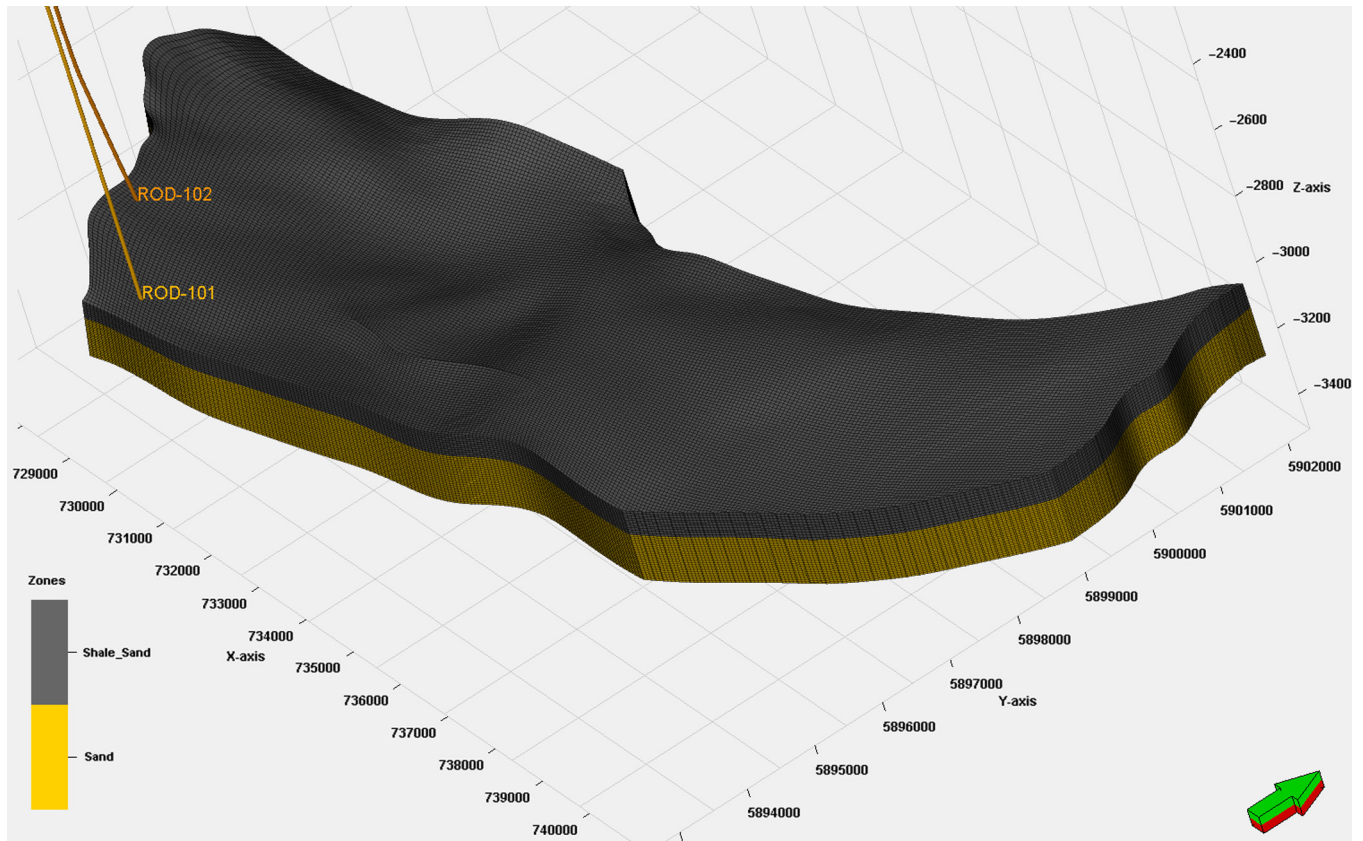**Figure 3.** Top Rotliegend depth map. After NAM (2005).

Figure 4. Main fault block of the Roden gas field reservoir model. Grey zone represents the shaly sand interval, while the yellow zone represents the sand interval.

the Petrel E&P Software Platform 2017.2 (Figure 4). Dynamic modelling has been carried out using the Eclipse 100 (2018.1) Reservoir Simulator.

As the main purpose of the simulations is to gain insight into the sensitivities of various production and reservoir parameters that have an impact on the potential synergy, no history match has been made with historical production data and only the ROD-102 well has been used. Tested sensitivities are:

1. Horizontal distance (250, 500 and 750 m) of the geothermal producer with regard to the gas–water contact (GWC);
2. Horizontal distance (1000, 1500 and 2000 m) of the geothermal injector with regard to the geothermal producer;
3. Flow rates (100, 150, 200 and 250 standard cubic metres per hour ($Sm^3 h^{-1}$)) of the geothermal doublet;
4. Flow rates (800,000 and 1,200,000 $Sm^3 d^{-1}$) of the gas producer ROD-102;
5. Permeability (homogeneous, doubled homogeneous, trend and inversed trend);
6. Aquifer support (limited aquifer and strong aquifer);
7. Timing of the start of geothermal exploitation.

In all scenarios the reference model of the Roden field has been used for comparison, unless noted otherwise. For each alternative development scenario a separate base case, referring to the gas production only, is defined. This base case is used as a reference for the specific scenario it belongs to.

Simulations are set to start at 1 January 1977 and run for 40 years until 1 January 2017. In all sensitivity scenarios apart from no. 7, geothermal and gas production start simultaneously.

For every scenario two graphs are presented: (a) cumulative gas production vs geothermal flow rate and (b) bottom hole pressure (BHP) vs year. Within the first graph the resulting cumulative gas production with respect to the imposed geothermal flow rate (100, 150, 200 and 250 $Sm^3 h^{-1}$) for (minimal) four geothermal well configurations is shown. Note that the resulting cumulative gas production of the scenario-specific base case (only gas production) is shown at a geothermal flow rate of 0 $Sm^3 h^{-1}$. In the second graph the BHP is plotted against the year of production. Here the base case of the reference model is given, with the base case of the specific scenario and the most extreme (low and high) results. Results of all other simulations are plotted between these low and high extreme outcomes. The total amount of gas produced and a comparison with base case values of every simulated scenario are given in the Appendix.

As many scenarios are presented in this paper, the methodology and the results are combined to improve readability. For each (alternative) scenario the set-up is explained, followed by its results and their sensitivity to the parameter settings.

The reference model

Methodology
The reservoir model outlines the main fault block of the Roden gas field and the connected aquifer. It comprises two reservoir intervals: an upper shaly sand interval, based on the ROCLT and shaly upper part of the ROSL, and a lower sand interval, based on the lower part of the ROSL. Reservoir properties of both intervals were determined from a petrophysical evaluation of the ROD-101(-S2), ROD-102 and ROD-201-S1 wells and are summarised in Table 1.

Table 1. Reservoir properties resulting from the petrophysical analysis

Interval	Avg Gross (mTVT)	Avg Net (mTVT)	N/G (%)	Avg PHIE[a] (%)	Avg Perm (mD)	Kv/Kh[b] (-)
Shaly sand	55	19.8	36	10	10	0.01
Sand	150	135	90	15	90	0.01

[a]Effective porosity.
[b]Vertical to horizontal permeability ratio.

Table 2. Gas composition used in reservoir simulations

Composition	Concentration (mole fraction)
Methane (C_1)	0.8119
Ethane (C_2)	0.0411
Propane (C_3)	0.0155
Iso-butane (iC_4)	0
Normal-butane (nC_4)	0.0068
Iso-pentane (iC_5)	0
Normal-pentane (nC_5)	0.0025
Hexanes (C_6)	0.0013
Heptanes plus (C_{7+})	0.0009
Hydrogen sulphide (H_2S)	0
Carbon dioxide (CO_2)	0.01
Nitrogen (N_2)	0.11

Table 3. Relative permeability input parameters

Parameter	Value
Critical gas saturation (S_{gcr})	0.05
Corey gas exponent (C_g)	3
Relative permeability of gas at minimum water saturation ($K_{rg}@S_{wmin}$)	0.9
Minimum water saturation (S_{wmin})	0.2
Critical water saturation (S_{wcr})	0.22
Corey water exponent (C_w)	6
Relative permeability of gas at residual oil saturation ($K_{rw}@S_{orw}$)	0.4
Relative permeability of water at a saturation value of unity ($K_{rw}@S = 1$)	1

Table 4. Capillary pressure (P_{cgw}) versus water saturation (S_w)

S_w	P_{cgw}
0.2	2.0
0.4	0.8
0.6	0.4
0.8	0.1
1.0	0.0

The properties are homogeneous for each layer, unless noted otherwise.

The top of the model ranges from 2850 to 3280 m true vertical depth (TVD). Boundary faults are considered to be sealing, whereas internal faults are completely open to flow. Cell size of the grid is set to 50×50 m horizontally. As layering is proportional to the thickness, cell height varies between 3.5 and 8.5 m.

At the GWC (3021 m TVD) the temperature and pressure are 102°C and 345 bar, respectively. A gas density of 0.816 kg m^{-3} has been used; its composition is given in Table 2. Gas formation volume factor and gas viscosity change with pressure, based on JP Spivey & WD McCain, Jr (unpublished report, 2003) and Carr et al. (1954) respectively. Formation water salinity is 200,000 ppm, with a water density of 1166 kg m^{-3}, a viscosity of 0.4960 cP and a compressibility of 3.056E-5 1/bar. The relative permeability curves of gas and water were modelled using the Corey correlation, with the input values given in Table 3. Capillary pressure is given in Table 4. Rock compressibility is modelled using the Newman equation (Newman, 1973), assuming consolidated sandstones.

The static gas initially in place (GIIP) of the reference model is 8.5×10^9 Sm^3. The gas production well ROD-102 is completed and perforated 68 m in the upper part of the gas cap, 40 m above the GWC. Only one casing of 6-5/8″ diameter is used in this well during the simulations. For most simulations gas production was fixed to 800,000 Sm^3 d^{-1}, with a maximum water-to-gas ratio (WGR) of 0.00025 Sm^3 Sm^{-3} (200 Sm^3 d^{-1} water production per 800,000 Sm^3 d^{-1} gas production). When the simulation reached the maximum WGR, the well was shut in. The minimum BHP was constrained at 15 bar; the gas production rate is adjusted to maintain this minimum BHP threshold.

Results

In the base case scenario (without a geothermal doublet), the ROD-102 well produces gas at a rate of 800,000 Sm^3 d^{-1} with a gradually decreasing BHP (Figure 5). The first production of water occurs halfway through 1986, nine years after the start of production. Water production rate increases exponentially, while the decrease in BHP becomes even more substantial. In 1993 ROD-102 is shut in, 16 years after the start of production, having produced 4.68 BCM of gas (Figure 5).

Sensitivity to geothermal well configuration

Methodology

In order to test the impact of the geothermal well configuration on total gas production in the reference model, multiple scenarios are defined using varying horizontal distances between the GWC and geothermal producer (250, 500 and 750 m; see Figure 6). Simultaneously the horizontal distance between the geothermal producer and -injector is set to alternate between 1000, 1500 and 2000 m for each aforementioned distance between the GWC and the geothermal producer (Figure 6). For each set of distances, the flow rate of the geothermal doublet is varied between 100, 150, 200 and 250 Sm^3 h^{-1} (respectively 2400, 3600, 4800 and 6000 Sm^3 d^{-1}). A total of 24 scenarios have been simulated. The geothermal producer and injector are oriented perpendicular to the GWC and parallel to the ROD-102 gas producer. Both geothermal wells are represented as vertical wells, both having a casing $8\frac{5}{8}″$ in diameter which is perforated over the entire reservoir interval. The minimum BHP was constrained at 100 bar; the flow rate of the geothermal wells is adjusted to maintain this 100 bar.

The results of these simulations are compared with the base case scenario of the reference model, i.e. having no active geothermal system.
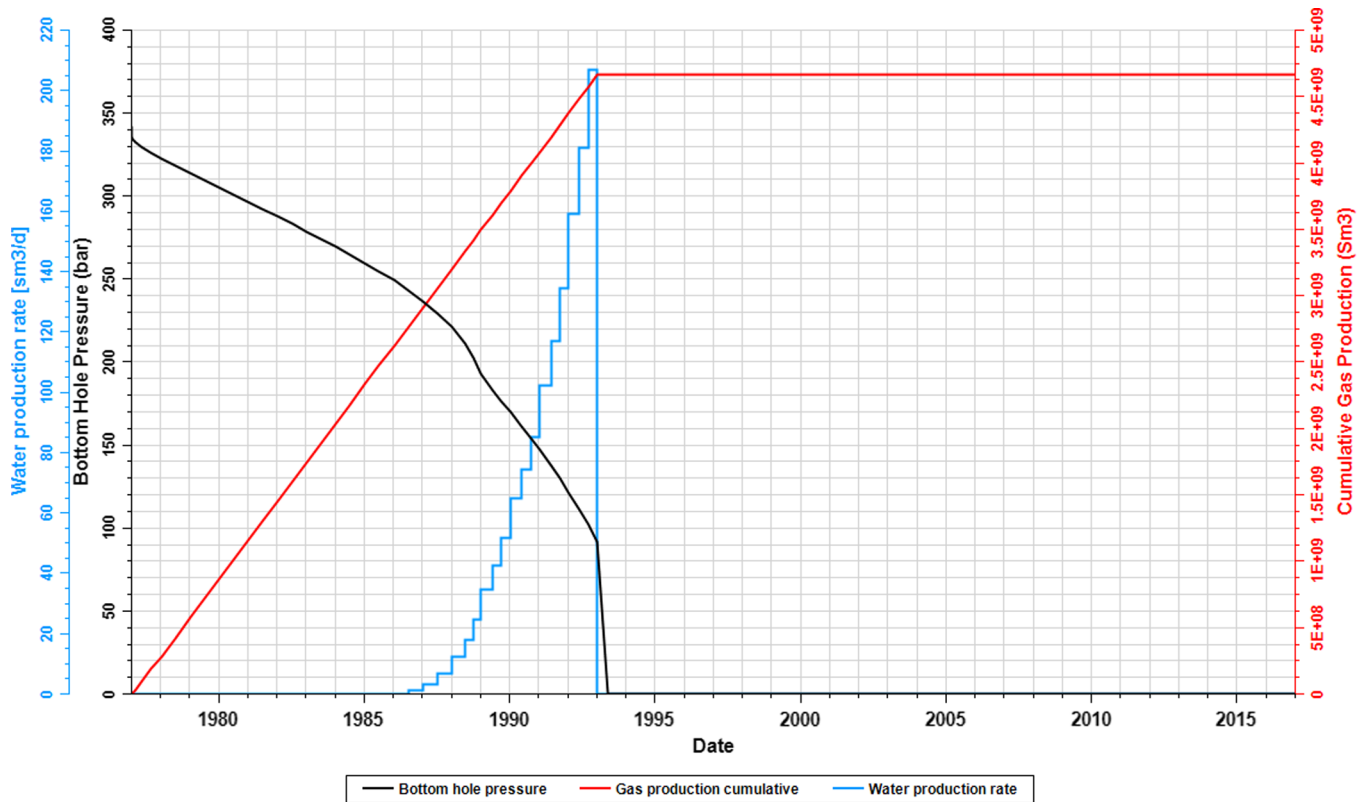
Figure 5. Results of the base case simulation: cumulative gas production, water production rate and bottom hole pressure of ROD-102. Note that the BHP becomes 0 bar as registration is stopped at cessation of production.
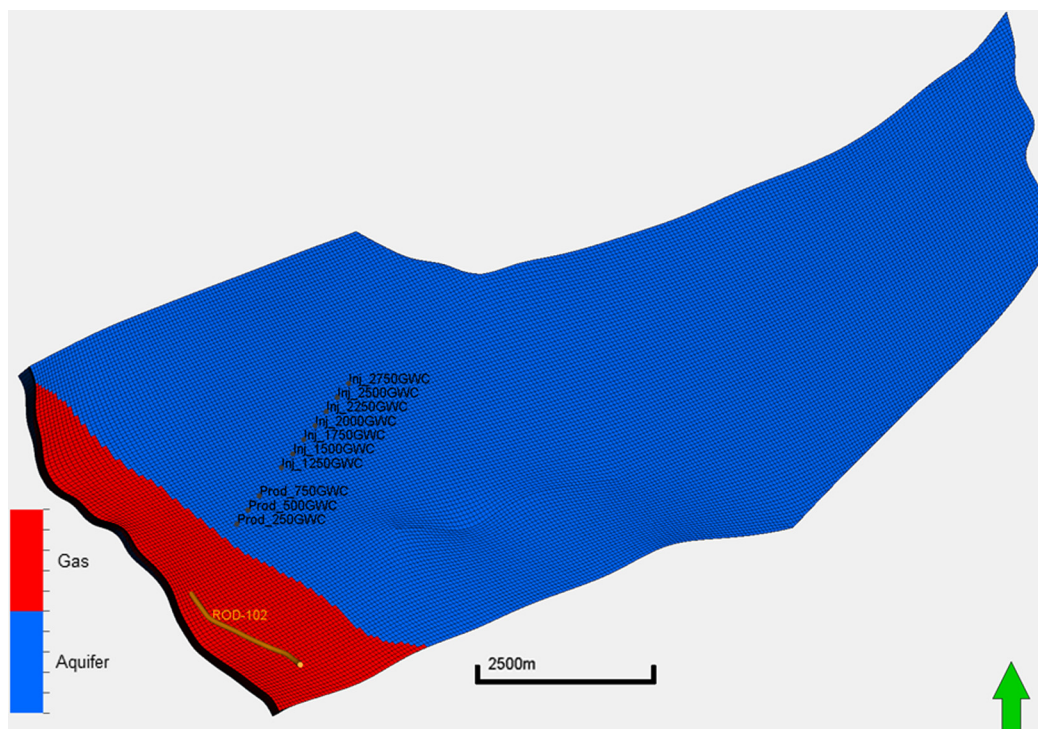

Figure 6. Map view of the main fault block of the Roden gas field with the initial GWC. Multiple geothermal well emplacements used in the sensitivity analysis are presented. Horizontal distance relative to the GWC is noted in the label.

Results

For every geothermal well configuration scenario an improved total gas production in ROD-102, compared with the reference model, is shown (Table A1 in the Appendix; Figure 7). The geothermal well configuration resulting in the highest cumulative gas production has a geothermal producer at 250 m from the GWC, the geothermal injector 2000 m from the geothermal producer, and a geothermal flow rate of 250 Sm^3 h^{-1}. The postponement of water breakthrough
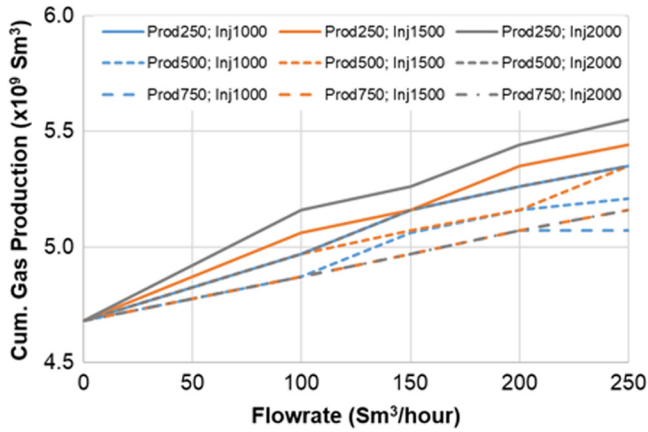
Figure 7. Results of sensitivity analysis of well configuration on cumulative gas production of ROD-102, with varying geothermal producer and -injector distances and geothermal flow rates using the reference model.

in ROD-102 is also reflected in the BHP (Figure 8). Synchronously, the BHP of the geothermal producer and geothermal injector decreases at a more or less similar rate to the ROD-102 well. When ROD-102 shuts in, the BHP in the geothermal wells stabilises and remains constant (Figure 8). For both production systems, the BHP constraint is not reached.

Increasing the distance of the geothermal producer with regard to the GWC leads to a decrease in total gas production (Figure 7), but an increase in BHP for the geothermal producer (Figure 8A). The opposite occurs when increasing the distance of the geothermal injector with regard to the geothermal producer and thus the GWC: total gas production increases (Figure 7) while the BHP in the geothermal producer decreases (Figure 8B). Enlarging the geothermal flow rate results in a more or less linear increase of total gas production (Figure 7).

Sensitivity to production rate of the ROD-102 well

Methodology
The flow rate of the ROD-102 gas production well is increased from 800,000 $Sm^3 \, d^{-1}$ to 1,200,000 $Sm^3 \, d^{-1}$ in order to test the effect of higher flow rates of the gas producer on the potential synergy. An alternative base case scenario is simulated to be used as a reference for the scenarios including geothermal wells. Sixteen out of the 24 geothermal well configurations described in the previous section are used. The WGR is lowered to 0.000167 $Sm^3 \, Sm^{-3}$ in order to maintain the 200 $Sm^3 \, d^{-1}$ water production limit.

Results
Increasing the gas flow rate to 1,200,000 $Sm^3 \, d^{-1}$ and having no geothermal exploitation leads to a lower cumulative gas production of 4.28 BCM (Table A2 in the Appendix; Figure 9A) compared to the reference model. Water breakthrough starts in 1982, ROD-102 shutdown in 1986. The addition of the geothermal system again enhances total gas production owing to a delay in water breakthrough (Table A2 in the Appendix; Figure 9A); the relative increase due to the geothermal system is slightly higher than in the reference model. The higher gas flow rate results in a more rapid decrease of BHP compared to the base case gas flow of 800,000 $Sm^3 \, d^{-1}$ (Figure 9B).

Increasing the horizontal distance of the geothermal producer with respect to the GWC shows a similar behaviour in total gas
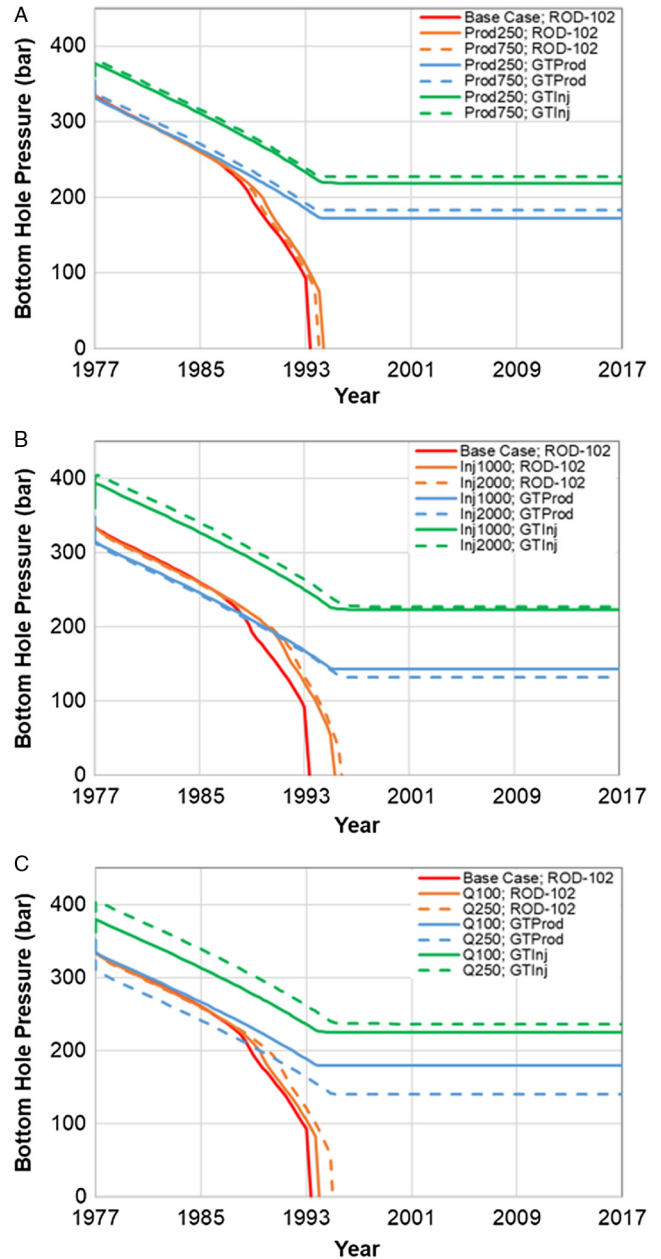

Figure 8. Comparison of bottom hole pressures of ROD-102, geothermal producer and -injector for: (A) different geothermal producer distances, with geothermal injector at 1000 m and geothermal flow rate Q = 100 $Sm^3 \, h^{-1}$; (B) different geothermal injector distances, with geothermal producer at 250 m and Q = 200 $Sm^3 \, h^{-1}$; (C) different geothermal flow rates, with geothermal producer at 500 m and -injector at 1000 m.

production (Figure 9A) compared with the reference model (Figure 7A). Increasing the distance of the geothermal injector and having the geothermal producer at 250 m from the GWC also shows a comparable rise in total gas production to that in the reference model. However, with the geothermal producer at 500 m, increasing the distance of the geothermal injector does not show (a significant) change in total gas production (Figure 9A). With an increased gas production rate the highest gas recovery increase is shown by the synergy scenario with a geothermal producer at 250 m from the GWC, the geothermal injector 2000 m from the geothermal producer and a geothermal flow rate of 250 $Sm^3 \, h^{-1}$.
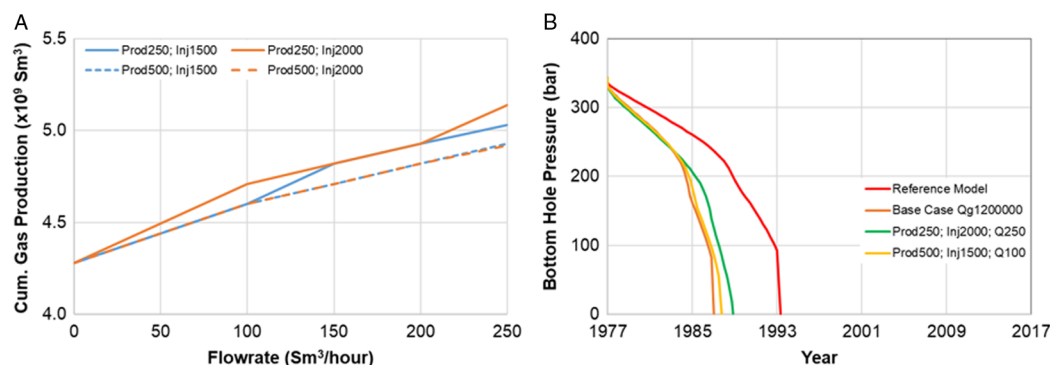
Figure 9. Results of sensitivity analysis of well configuration and gas flow rate 1,200,000 Sm³ d⁻¹ on cumulative gas production of ROD-102. (A) Varying geothermal producer and -injector distances and geothermal flow rates; (B) bottom hole pressure.
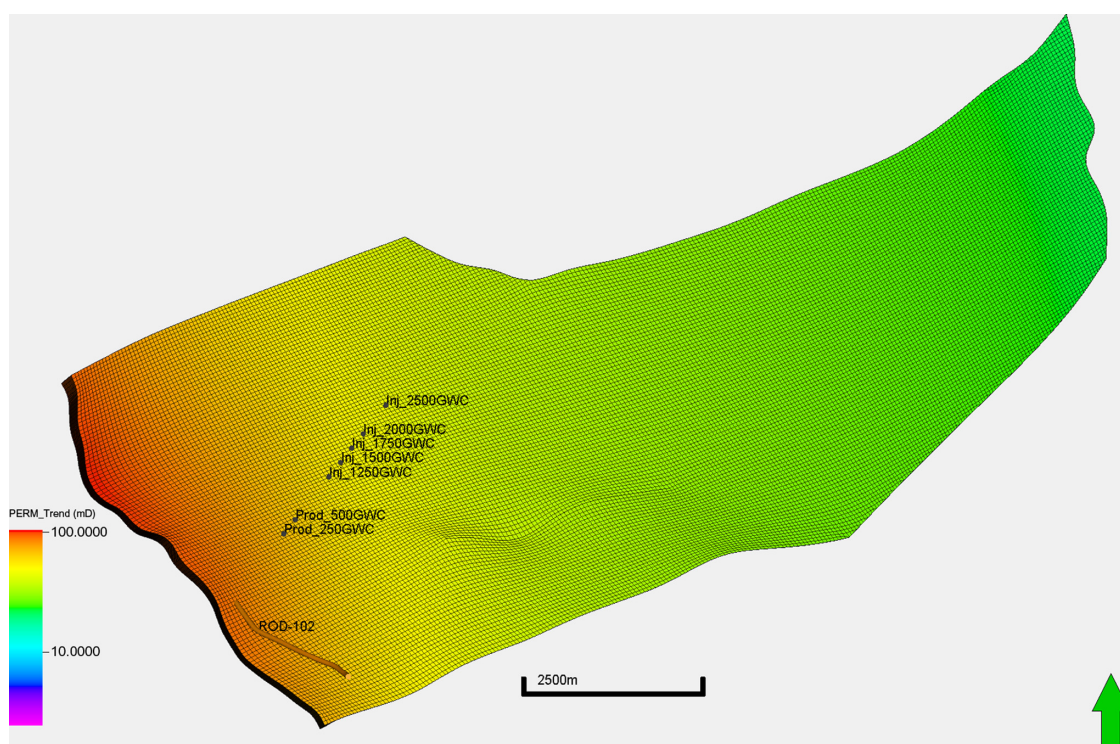

Figure 10. Map view of the main fault block of the Roden gas field with a decreasing permeability trend from the ROD-102 well towards the geothermal wells.

Sensitivity to reservoir permeability

Methodology
The aforementioned 16 geothermal well configurations are used to assess three different permeability grids. The first grid considers a doubling of the original permeability grid (10 and 90 mD) in both intervals to 20 mD (shaly sand interval) and 180 mD (sand interval). The vertical reservoir permeability is also doubled. In the second grid the homogeneous permeability distribution is replaced by a trend. The sand interval has a permeability of 90 mD at the ROD-102 well, which decreases towards ±67 mD at the geothermal producer and ±50 mD at the geothermal injector (Figure 10). The permeability trend values for the shaly sand interval are 10 mD towards 7.5 mD and 5.5 mD respectively. The third grid considers an inversed permeability trend. Here the sand interval has a permeability of 90 mD at the outermost possible geothermal injector, which decreases towards ±58 mD at the geothermal producer and 45 mD at the ROD-102 well (Figure 11). For the

shaly sand interval the trend values range from 10 mD to 6.5 and 5 mD respectively. For each of the alternative permeability grids, a new base case scenario is simulated for comparison.

Results
Doubling the reservoir permeability, and having no geothermal exploitation, results in a higher total gas production (4.87 BCM) in comparison with the reference model (Table A2 in the Appendix). ROD-102 is closed-in in late 1993, with water breakthrough starting in 1987. While the addition of the geothermal doublet again results in increased total gas production, the relative increase is smaller than in the reference model (Table A2 in the Appendix; Figure 12A). The increased permeability causes the BHP to decrease more slowly during gas production (Figure 12B).

As with previous sensitivity analysis, the change in distance of the geothermal producer changes the total gas production. However, with increased permeability the change in distance of
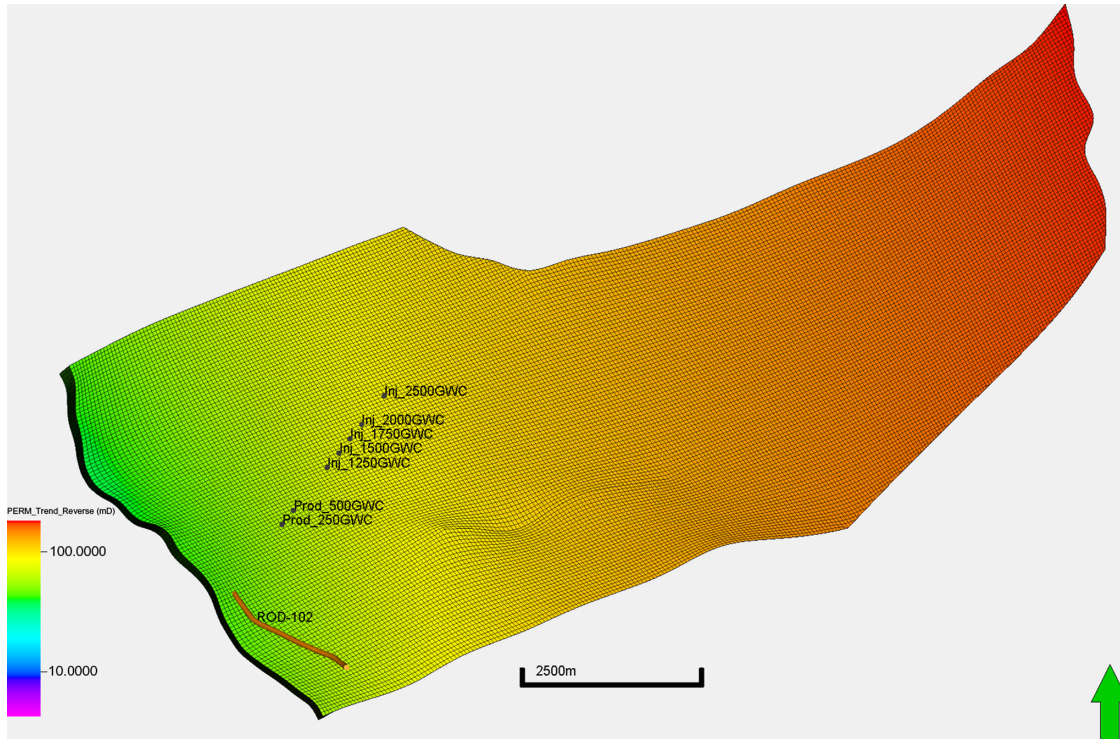
Figure 11. Map view of the main fault block of the Roden gas field with an increasing permeability trend from the ROD-102 well towards the geothermal wells.
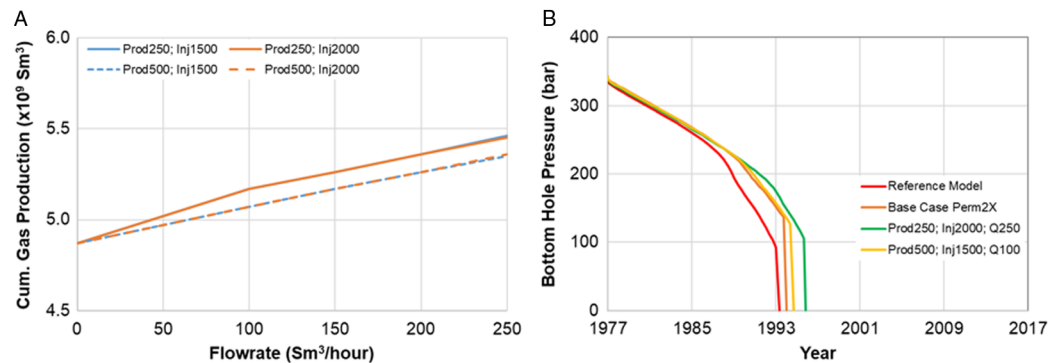

Figure 12. Results of sensitivity analysis of well configuration and reservoir permeability doubled on cumulative gas production of ROD-102. (A) Varying geothermal producer and -injector distances and geothermal flow rates; (B) bottom hole pressure.

the geothermal injector has no effect on the total amount of gas produced (Figure 12A). This is also shown with having the geothermal injector at 1500 m from the geothermal producer resulting in the highest increase in gas recovery versus the geothermal injector at 2000 m.

A reservoir permeability that decreases away from ROD-102 shows a slight increase (4.78 BCM) in total gas production, with no geothermal doublet active, when compared to the reference model (Table A2 in the Appendix; Figure 13A). When the geothermal system is introduced, the most significant differences in total gas production can be attributed to the flow rate of the doublet. At a flow rate of 100 m³ h⁻¹ the change in distance of the injector has no impact; increasing the flow rate makes this change more apparent. With higher flow rates the relative increase of total gas production is reduced (Figure 13A). The BHP behaviour is not very different to that in the reference model (Figure 13B). The optimum geothermal well configuration in this scenario is having the geothermal producer at 250 m from the GWC, the

geothermal injector 2000 m from the geothermal producer and a geothermal flow rate of 250 Sm³ h⁻¹ (Table A2 in the Appendix).

The reservoir permeability decreasing from the geothermal injector towards ROD-102 shows the opposite behaviour to that described above. Total production of gas, without geothermal wells, is less (4.29 BCM) than in the reference model (Table A2 in the Appendix; Figure 14A). The effect of altering the geothermal injector distance is subordinate to the effect of changing the distance of the geothermal producer with regard to the GWC. This difference becomes more pronounced with higher geothermal flow rates (Figure 14A). The BHP of ROD-102 shows that the minimum pressure constraint of 15 bar is reached in all synergy scenarios before ROD-102 is shut in due to water breakthrough (Figure 14B). A geothermal well configuration, where the geothermal producer is at a distance of 250 m from the GWC, the geothermal injector 1500 m from the geothermal producer and having a geothermal flow rate of 250 Sm³ h⁻¹, results in the highest increase in gas recovery.
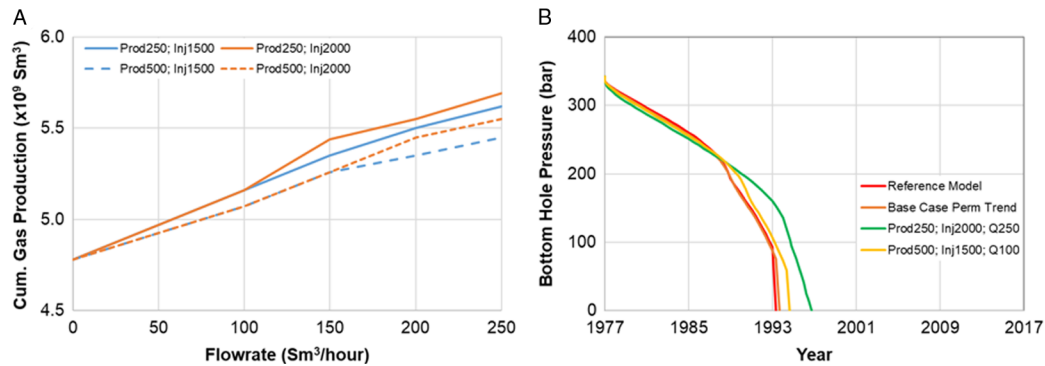
Figure 13. Results of sensitivity analysis of well configuration and reservoir permeability trend on cumulative gas production of ROD-102. (A) Varying geothermal producer and -injector distances and geothermal flow rates; (B) bottom hole pressure.

Figure 14. Results of sensitivity analysis of well configuration and reservoir permeability trend inversed on cumulative gas production of ROD-102. (A) Varying geothermal producer and -injector distances and geothermal flow rates; (B) bottom hole pressure.
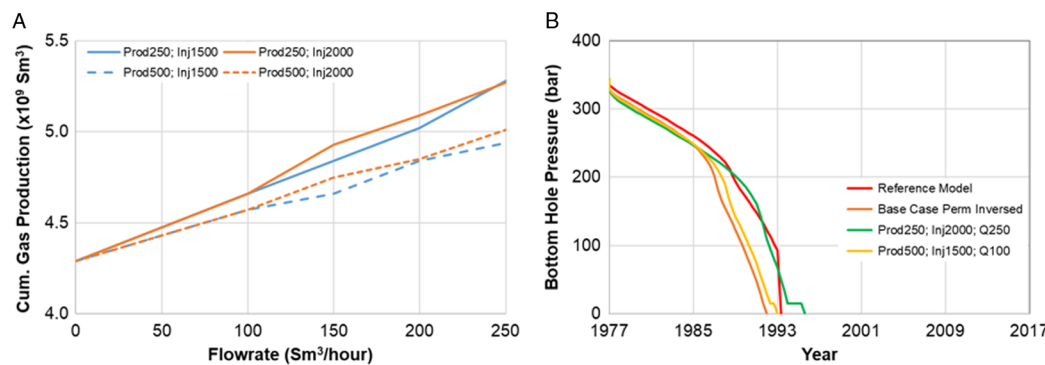
Sensitivity of aquifer support

Methodology
Van der Meulen (2016) demonstrated that the absence of a proper aquifer obstructs synergy between hydrocarbon- and geothermal energy production due to a severe drop of reservoir pressure and consequently both systems interfering with one another. To mimic this behaviour, the aquifer size of the Roden reservoir model is reduced to nearly a third (Figure 15). Furthermore, another scenario is tested which assumes a very strong aquifer drive. This is achieved by introducing a pressure boundary condition in the water zone on the edges of the reservoir model. In both sensitivity analyses the previously used 16 geothermal well configurations are used to test the impact of the aquifer support on the total gas production.

Results
Limiting the size of the aquifer decreases the total gas production, with no geothermal doublet active, to 3.69 BCM when compared with the reference model (Table A2 in the Appendix; Figure 16A). Water breakthrough starts in 1985. The addition of an active geothermal doublet shows that altering both geothermal producer and -injector distances has a limited effect. The increase of geothermal flow rate also shows a limited increase of total gas production (Figure 16A). With the limited aquifer, the BHP decreases quite rapidly and the minimum BHP constraint of 15 bar is reached (Figure 16B). The flow rate of ROD-102 is lowered in order to maintain this minimum BHP.

The presence of a strong aquifer drive also leads to a lower cumulative gas production (3.70 BCM) when compared with the reference model (Table A2 in the Appendix; Figure 17A). The effect of changing the distance of the geothermal injector is less significant than the effect of changing the geothermal producer's distance. Increasing the geothermal flow rate leads to a more or less

linear increase of total gas production (Figure 17A). The most significant effect of the strong aquifer drive is the reduced decrease of BHP compared with the reference model and the limited aquifer (Figure 17B). Before the start of water breakthrough the BHP remains close to its initial steady-state pressure.

For both scenarios, a geothermal well configuration with the geothermal production well at 250 m from the GWC, geothermal injection well 2000 m from the geothermal producer and a geothermal flow rate of 250 Sm³ h⁻¹ leads to the highest gas recovery increase (Table A2 in the Appendix).

Sensitivity to the timing of geothermal production start

Methodology
With many gas fields in the Netherlands being well underway in their production life, it is interesting to see what the (theoretical) impact is of geothermal exploitation on the potential synergy in the various stages of gas production. Using the original reference model, simulations are run to test this effect given the following timings of geothermal production:

1. Simultaneous start of gas- and geothermal production;
2. Halfway before water breakthrough;
3. At start of water breakthrough;
4. When ROD-102 closes in due to excessive water production, with gas production restarting 4 years later;
5. When ROD-102 closes in due to excessive water production, with gas production restarting 10 years later.

The geothermal well configuration used to test these five scenarios includes a geothermal producer at 500 m from the GWC, the geothermal injector at 2500 m from the GWC and a flow rate of 250 Sm³ h⁻¹.
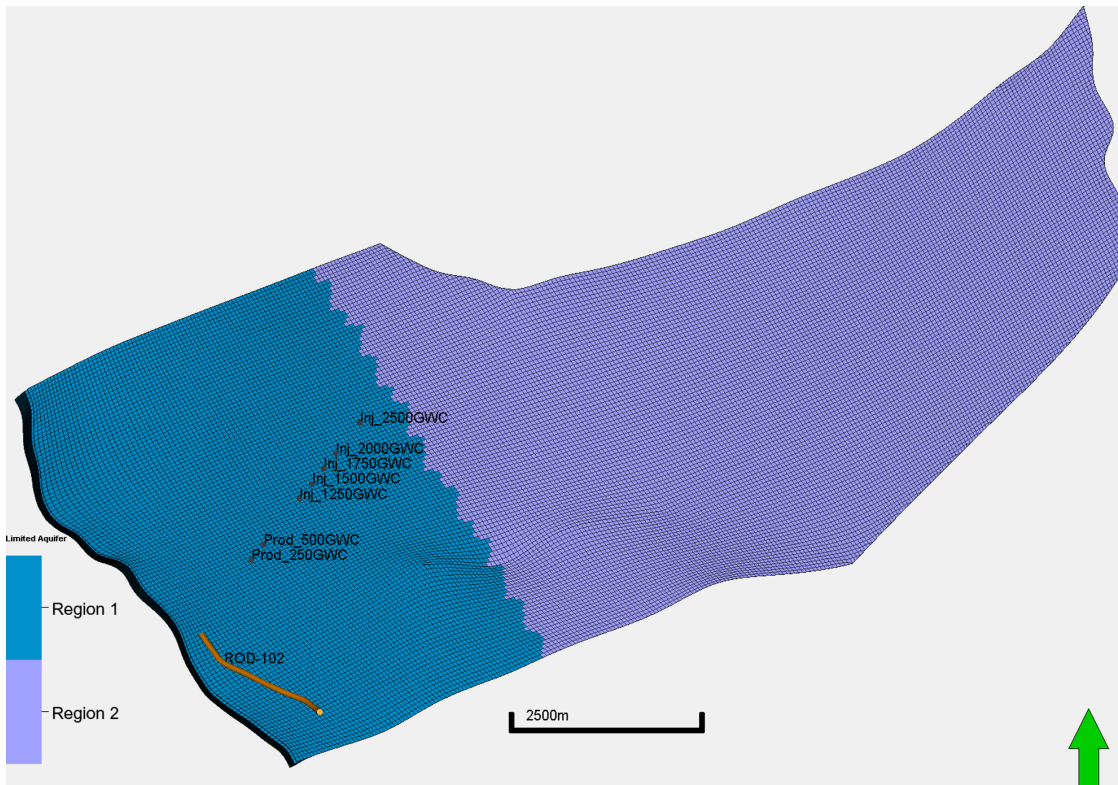
Figure 15. Map view of the main fault block of the Roden gas field with a reduced aquifer size. Region 1 contributes to flow, region 2 does not.
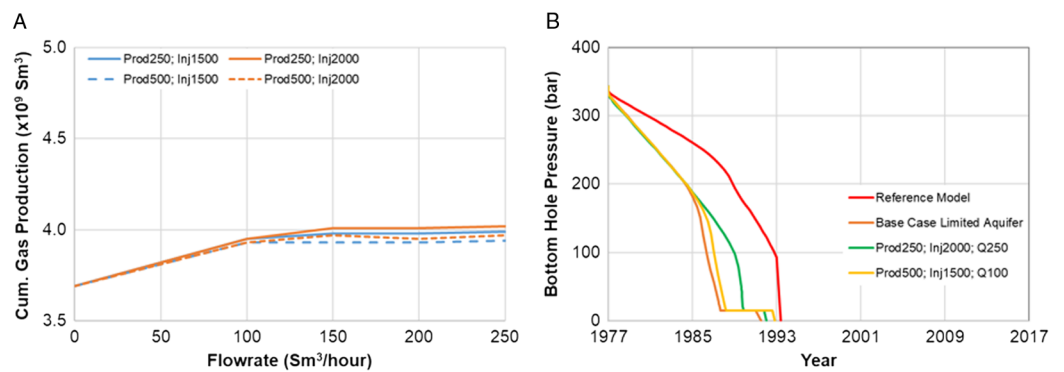
Figure 16. Results of sensitivity analysis of well configuration and aquifer size reduced on cumulative gas production of ROD-102. (A) Varying geothermal producer and -injector distances and geothermal flow rates; (B) bottom hole pressure.
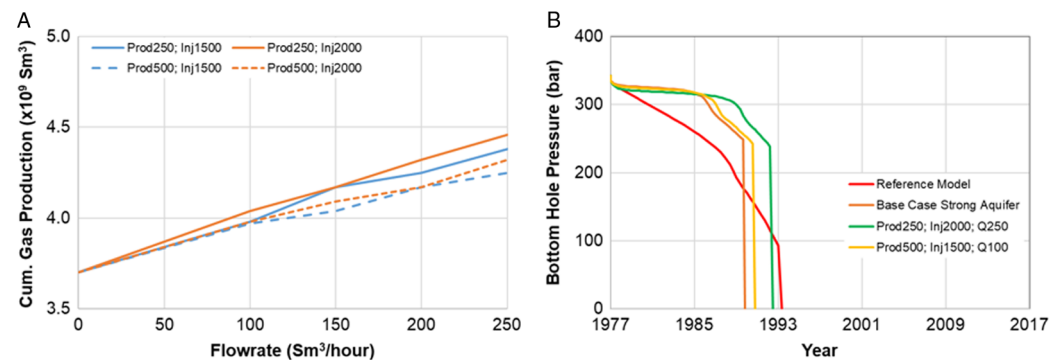
Figure 17. Results of sensitivity analysis of well configuration and increased aquifer drive on cumulative gas production of ROD-102. (A) Varying geothermal producer and -injector distances and geothermal flow rates; (B) bottom hole pressure.

Figure 19. Bottom hole pressures of the geothermal production well for different scenarios. Distance geothermal production well at 250 m, geothermal injector at 1500 m and flow rate is 250 Sm^3 h^{-1}.

Figure 18. Results of sensitivity analysis of the timing of starting geothermal exploitation on cumulative gas production of ROD-102. Distance geothermal producer at 250 m, geothermal injector at 2000 m and flow rate is 250 Sm^3 h^{-1}. (A) Start geothermal exploitation before ROD-102 shut-in; (B) start geothermal exploitation after ROD-102 shut-in, with gas production resuming in later stages.

Figure 20. Gas production rate of co-produced gas in geothermal production well for different scenarios. Distance geothermal production well at 250 m, geothermal injector at 1500 m and flow rate is 250 Sm^3 h^{-1}.

Results

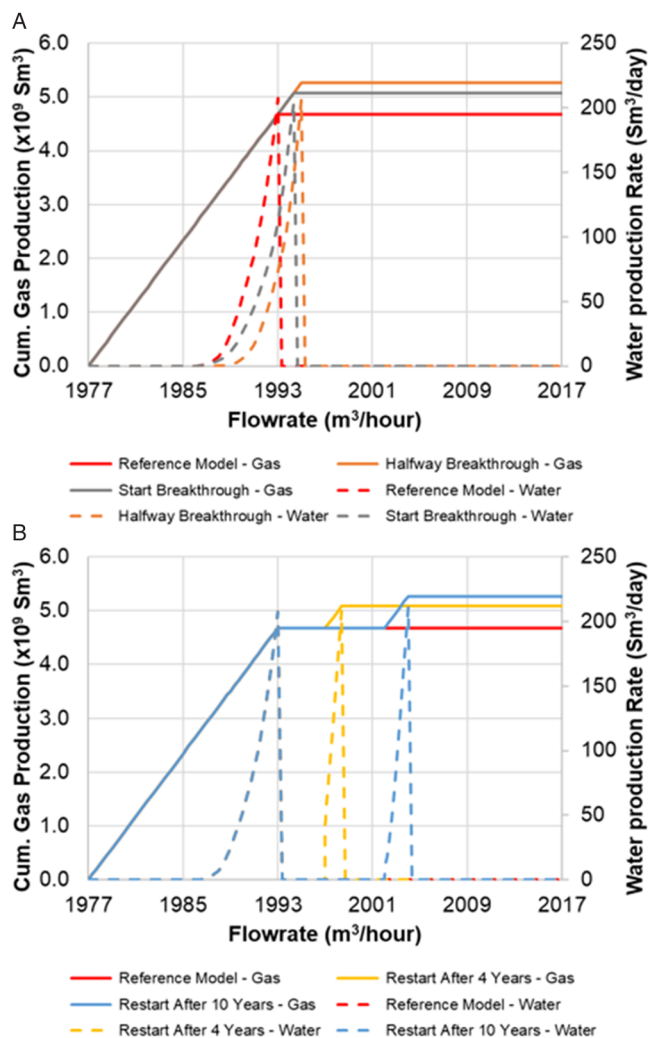The *timing* scenarios show that geothermal production in the water leg in later stages of gas production is still beneficial to the cumulative gas production (Table A3 in the Appendix). The addition of a geothermal doublet before the close-in of ROD-102 can still affect the encroaching water table significantly (Figure 18A). Geothermal exploitation after the shut-in of the gas well can still have an impact when gas production is resumed afterwards; higher gas recoveries are obtained the longer geothermal production occurs (Figure 18B).

Other observations

Bottom hole pressure in geothermal producer

In nearly all scenarios the geothermal wells are affected by the decrease in reservoir pressure, subsequently leading to lower BHPs in the geothermal wells (Figure 19). In a limited aquifer scenario, the impact of the pressure drop is largest and the minimum BHP constraint of 100 bar is reached. This causes the geothermal flow rate to be lowered accordingly. The scenario with a

strong aquifer drive shows that the BHP is barely affected by the gas production, and it quickly restores to the initial BHP once gas production ceases.

Co-production of natural gas in geothermal producer

In many scenarios the geothermal producer with higher flow rates also produces gas along with the produced water (Tables A1 and A2 in the Appendix). The amount of gas being produced strongly depends on the reservoir setting, with the reservoir models with trends showing the highest gas rates (Figure 20). With higher gas production rates the geothermal producer only starts to produce gas once ROD-102 closes in. In a strong aquifer drive setting, there is very little gas production compared with other scenarios.

Economics

Methodology

The most prolific well configuration, aiming for high geothermal power output and a coefficient of performance (COP) higher than 10 in the reference model, is used to calculate the economics of the geothermal system. The potential geothermal power is determined using DoubletCalc 1.4.3 software (Van Wees et al., 2012). For both geothermal wells a skin of −1 is added in order to mimic deviated

wells. The outcome of the DoubletCalc scenario is used to calculate the economics of the geothermal system, based on the ThermoGIS calculation method (Van Wees et al., 2012; TNO, 2018). Heat price is based on the gas price, being €0.014 kWh^{-1} and €0.016 kWh^{-1} respectively (Lensink & Van der Welle, 2018). Two economic scenarios using the Net Present Value are calculated: one with and one without the feed-in premium for renewable energy (SDE+ subsidy) from the Dutch government. The reference price of the subsidy is €0.053 kWh^{-1} (Lensink et al. 2018). The lifetime of the geothermal doublet is set to 30 years.

The cost of drilling and completing ROD-102 is estimated to be €10 million (M) based on the method of Lukawski et al (2014), and assuming a dollar–euro conversion rate of 0.69 in 2009 and a well cost multiplier of 1.5. Numerous (confidential) onshore gas field developments are used to determine the CAPEX (Capital Expenditures) and OPEX (Operation Expenditures). CAPEX, including surface facilities and pipelines, are estimated at €15M. The total initial investment thereby becomes €25M. Annual OPEX is based on a variable gas OPEX of €0.033 Sm^{-1}. Royalties are set at 12%, tax at 25% and depreciation is set at 10 years. The economics of the reference model and the synergy scenario with the most prolific well configuration are calculated and compared. Based on the outcome, it is determined how much of the additional profit can be used to fund the geothermal system to break-even level.

Results

Using the DoubletCalc software the most profitable geothermal well configuration is deduced, assuming the reference model: geothermal producer at 250 m, geothermal injector at 2000 m and a flow rate of 250 Sm^3 h^{-1}. To account for the decreasing reservoir pressure due to gas production, the average reservoir pressure (265 bar at the producer and 300 bar at the injector) is used in DoubletCalc. Production pump depth (ESP) is increased from 700 m to 1500 m and pump pressure difference increased to 163 bar. The resulting base case geothermal power is 20.99 megawatts (MW), with a COP of 11.3 (Figure 21). This result is used to calculate the NPV over time, which shows that after 30 years of production with a SDE+ subsidy the NPV is €26.8M, but having no subsidy results in a negative NPV of €−41.1M (Figure 22A).

The total gas production of the base case is 4.68 BCM, with production from ROD-102 ending at the start of 1993. The resulting NPV after 16 years of production is €257.5M (Figure 22B). Synergy, with the addition of a geothermal producer at 250 m, geothermal injector at 2000 m and geothermal flow rate at 250 Sm^3 h^{-1}, extends gas production in ROD-102 by 3 years. Total gas production is increased to 5.55 BCM, improving the NPV of the gas field after more than 18.5 years of gas production to €319M.

Discussion

The potential synergy between gas- and geothermal exploitation has been tested using a reservoir model of the Roden gas field. The sensitivity analyses on geothermal well configuration show that every configuration leads to a higher total gas production due to delay in detrimental water breakthrough. The position of both the geothermal producer and -injector combined with the geothermal flow rate is key to maximise the effect of synergy between gas- and geothermal production. Placing the geothermal producer closer to the GWC and the gas producer increases total gas production in ROD-102. While geothermal production has limited pressure effects on gas production, there is a significant pressure effect from gas production on geothermal production. The pump pressure in the geothermal production well has to be adapted following the decreasing reservoir pressure during gas production and possible repressurisation due to active aquifer effects after gas production has ceased. The required increase of pump pressure upon reservoir depletion leads to higher electricity usage and subsequently to a lower COP. In addition, more expensive pumps are required in support of the increased capacity. However, the reduced reservoir pressure also has a positive effect on the geothermal injection, as a lower pump pressure is required for injection.

With geothermal production close to the GWC, higher geothermal flow rates will also result in co-production of (free) natural gas. Free natural gas has the potential to hinder the overall production in the ESP, as is also often an issue for oil production. In this study the ratio of co-produced free gas and the produced water in the geothermal production well does not exceed 2.5%, thereby keeping the effect of free gas on the overall production very limited. So far no geothermal systems in the Netherlands co-produce free gas, yet formation water often contains dissolved gas which turns into free gas once it comes to the surface (MEA, 2018). The current average ratio for Dutch geothermal systems producing from the ROSL is more or less 0.3 Sm^3 natural gas per 1 Sm^3 of water produced. It is very likely that produced formation water from the water leg also contains dissolved natural gas, especially when a transition zone is present. This aspect has not been taken into account in the simulations and economic calculations of this study. Overall, both free and dissolved natural gas could have an added benefit for the geothermal project, either through gas sales and/or by providing power to the ESP in the geothermal production well, resulting in a reduction of the electricity costs of the pump.

The economics of conventional geothermal systems depend on an optimal distance between producer and injector. This is, among others, modelled in the DoubletCalc 1.4.3 software (Van Wees et al. 2012). On the one hand, a shorter distance increases the pressure gradient and thereby improves water production at the geothermal producer. On the other hand, a longer distance increases the lifetime of a geothermal system as breakthrough of cooler injected water at the geothermal production well is postponed. In the synergy scenarios, a greater distance between the geothermal wells will increase gas production. This benefit strongly outweighs the benefits of choosing a shorter distance for higher pressure gradients and improved geothermal power.

The sensitivity analyses with regard to increased gas flow rate, increased permeability, added permeability trends and limited- and strong aquifer support all show a positive effect on total gas production when a geothermal doublet is added. However, each setting shows different reactions to the geothermal exploitation on the gas production:

Increasing the flow rate of ROD-102 shows somewhat similar behaviour to the reference model, with the exception of increasing the injector distance to the geothermal producer at 500 m. The increased drop in reservoir pressure nullifies the pressure effect from geothermal injection at a distance of 2500 m or more from the GWC. More important is the effect of the lower reservoir pressure on the economic performance of the geothermal doublet. In this case a higher pump pressure would be required, resulting in higher costs for the geothermal system. While the relative increase in gas production due to synergy is higher than in the reference model, the absolute total gas production is lower. It is therefore important not only to find the optimal geothermal well configuration, but also to consider a proper gas production rate in order to correctly balance the gas- and geothermal production.

Geotechnics (Input)

Property	min	median	max
aquifer permeability (mD)	60.0	70.0	80.0
aquifer net to gross (-)	0.72	0.76	0.8
aquifer gross thickness (m)	200.0	215.0	230.0
aquifer top at producer (m TVD)	2766.0	3073.0	3380.0
aquifer top at injector (m TVD)	2922.0	3247.0	3572.0
aquifer water salinity (ppm)	210000.0	220000.0	230000.0

Property	value
number of simulation runs (-)	1000.0
aquifer kh/kv ratio (-)	1.0
surface temperature (°C)	10.0
geothermal gradient (°C/m)	0.031
[mid aquifer temperature producer (°C)]	0.0
inital aquifer pressure at producer (bar)]	265.0
[initial aquifer pressure at injector (bar)]	300.0
exit temperature heat exchanger (°C)	25.0
distance wells at aquifer level (m)	1500.0
pump system efficiency (-)	0.61
production pump depth (m)	2000.0
pump pressure difference (bar)	163.0
outer diameter producer (inch)	8.5
skin producer (-)	-1.0
skin due to penetration angle p (-)	0.0
pipe segment sections p (m AH)	1500.0,1600.0,3073.0
pipe segment depth p (m TVD)	1500.0,1600.0,3073.0
pipe inner diameter p (inch)	9.85,12.4,8.5
pipe roughness p (milli-inch)	1.8,1.8,1.8
outer diameter injector (inch)	8.5
skin injector (-)	-1.0
skin due to penetration angle i (-)	0.0
pipe segment sections i (m AH)	1500.0,1600.0,3247.0
pipe segment depth i (m TVD)	1500.0,1600.0,3247.0
pipe inner diameter i (inch)	9.85,12.4,8.5
pipe roughness i (milli-inch)	1.8,1.8,1.8

Geotechnics (Output)

Monte Carlo cases (stochastic inputs)	P90	P50	P10
aquifer kH net (Dm)	10.47	11.41	12.47
mass flow (kg/s)	65.54	77.6	90.79
pump volume flow (m³/h)	209.5	249.1	292.1
required pump power (kW)	1555.0	1848.7	2167.9
geothermal power (MW)	16.86	20.71	25.57
COP (kW/kW)	10.6	11.3	12.0
aquifer pressure at producer (bar)	265.0	265.0	265.0
aquifer pressure at injector (bar)	300.0	300.0	300.0
pressure difference at producer (bar)	34.93	40.51	44.06
pressure difference at injector (bar)	98.78	115.03	133.42
aquifer temperature at producer * (°C)	103.37	108.59	113.84
temperature at heat exchanger (°C)	100.74	105.94	111.28

base case (median value inputs)	value
aquifer kH net (Dm)	11.44
mass flow (kg/s)	78.13
pump volume flow (m³/h)	250.8
required pump power (kW)	1861.6
geothermal power (MW)	20.99
COP (kW/kW)	11.3
aquifer pressure at producer (bar)	265.0
aquifer pressure at injector (bar)	300.0
pressure difference at producer (bar)	40.02
pressure difference at injector (bar)	115.98
aquifer temperature at producer * (°C)	108.6
temperature at heat exchanger (°C)	106.0
pressure at heat exchanger (bar)	47.09

* @ mid aquifer depth

Figure 21. DoubletCalc 1.4.3 result. Both input and output are given; base case is used as input for economics.

With a higher reservoir permeability, a lower drawdown pressure is required in order to produce the imposed gas flow rate, which subsequently leads to a relatively higher BHP in ROD-102 and a relatively higher pressure in the reservoir. Furthermore, the lower drawdown pressure causes a slight delay in water production at the gas production well. This results in a higher total gas production. Due to this improvement, the relative synergetic effect on gas production in ROD-102 is less when the geothermal wells are active. Therefore, it can be deduced that a higher permeability does not necessarily lead to an increased effect by synergy. However, the slower decrease in reservoir pressure does have a positive effect on the required pump pressure of the geothermal production well, thereby improving the COP and thus the economics of the geothermal system.

The positive effect of a synergetic geothermal – natural gas development also depends on the presence of a permeability trend in the produced reservoir and its orientation relative to the flow paths towards the gas- and geothermal production wells. With an increasing reservoir permeability from the geothermal wells towards the gas production well, the preferred gas production flow path from ROD-102 is in the opposite direction to the GWC. While this situation leads to an increase in total gas production in the simulations, the relative impact on the geothermal exploitation is lower due to the fact that this trend results in
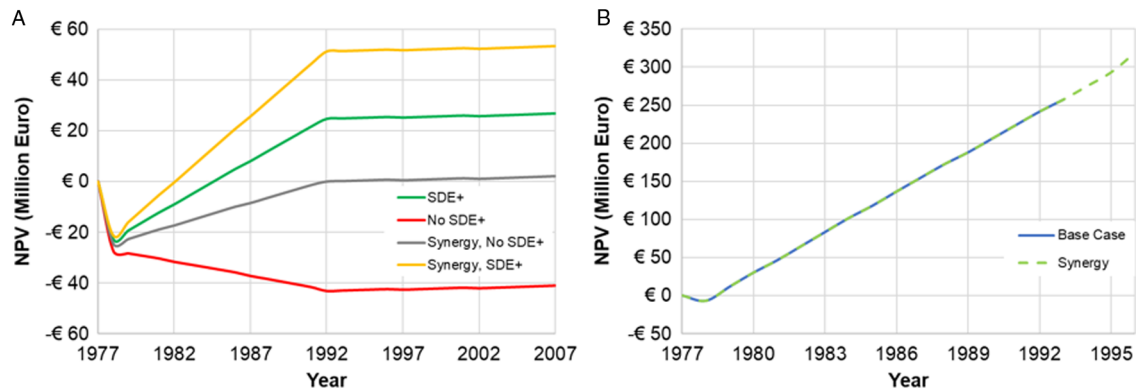
Figure 22. Net Present Value. (A) Different geothermal doublet economic scenarios. (B) Gas production with and without the geothermal doublet.

a lower permeability around the geothermal wells. Reversing this permeability trend results in an opposite behaviour, with reduced productivity in the gas well and better productivity in the geothermal well. Either way, in both permeability trend scenarios geothermal production enhances total gas production, yet a proper geothermal well configuration is needed to cope with the heterogeneous reservoir permeability.

The Roden gas field pressure data and simulation results suggest there is a combination of depletion drive and aquifer drive. Scenarios based on a more limited aquifer drive result in a significantly lower total gas production, while there is a larger drop in reservoir pressure. In these cases the positive effect from a geothermal system on total gas production also becomes less noticeable, especially when geothermal flow rate is increased. The lower reservoir pressure imposes a lower BHP at the geothermal producer, resulting in a reduced geothermal flow rate when the minimum constraint of 100 bar is reached. The same behaviour, albeit less pronounced, has been described by Van der Meulen (2016). A limited aquifer drive thus limits the mutual positive effects on gas- and geothermal production. A strong aquifer drive, on the other hand, increases the beneficial effects of a geothermal system near a gas producer. Although the aquifer drive lowers total gas production due to increased water production, the geothermal system does have a relatively stronger effect on cumulative gas production. Yet the most significant benefit is observed at the geothermal producer as the stronger aquifer drive keeps the BHP nearly constant. The maintenance of more or less constant hydrostatic pressure will reduce the costs of the ESP and required electricity while an increased pump pressure at hydrostatic pressure leads to an increase of geothermal power. Furthermore, a lower gas production rate would very likely result in a relative delay in water breakthrough, resulting in a higher recovery factor compared with the reference model. Optimisation of gas production, combined with synergy with geothermal exploitation, is therefore key.

The *timing* scenarios show that the installation of a geothermal doublet within the water leg at later stages of production can still be beneficial for the total gas recovery. More importantly, geothermal production near a closed-in gas field or where gas production is reduced due to excessive water production could raise the interest for redevelopment, depending on the duration of geothermal production.

In the investigated Roden case, the combined development of gas production and geothermal production leads to a profit of *c.* €319M, which is €61.5M higher than a gas-only production development. Without SDE+ subsidy for the geothermal doublet, *c.* €43.2M of the €61.5 million which is earned through the

production of extra natural gas may be used to finance the geothermal project at a break-even level after 15 years (Figure 22A). In this case *c.*€18.3M remains as net profit from the gas production. With a grant for SDE+ subsidy for the geothermal project, the geothermal project still has a CAPEX of €26.4M, which is regarded as a high-risk investment for geothermal operators. If the initial investment of €26.4M is financed by the revenues from extra gas production, a net profit of €35.1 remains. When the €26.4M CAPEX investment is paid back over a period of 15 years, the geothermal project reaches a NPV of €0 after 5 years of production, and a NPV of €53.3M after 30 years of production (Figure 22A).

It must be noted that this study considers two separate production facilities for the economic calculations. It is probably more efficient to combine both geothermal- and gas production in one production facility, thereby lowering initial CAPEX and annual OPEX. For instance, overhead costs will be reduced, as well as the combined purchase of materials for the facility. This will also present the possibility of increasing the power of the geothermal system by also using the co-produced hot formation water from the gas production well, while avoiding the costs of transporting the 'waste' formation water to a water disposal well. Furthermore, the joint development makes it easier and less costly to process and evacuate eventual natural gas that is co-produced in the geothermal production well. To the knowledge of the authors, a combined production facility has not been realised yet. Therefore, a (detailed) calculation of economics based on a reference case was not possible. Additionally, the authors have no access to essential data nor the required expertise to perform such detailed calculations.

Unlike the actual Roden gas field development, this study did not investigate any optimisations for the gas production strategy related to (excessive) water production. If this were taken into account, then the positive effects of a combined development with geothermal exploitation would possibly become even higher considering the expected increase in gas recovery. Also the repressurisation observed in the Roden field (87 bar pressure increase 10 years after cessation of production) has not been accounted for in any of the investigated scenarios. This should, however, have a positive impact on geothermal production as well.

The synergy between gas production and geothermal exploitation as described in this study can play a positive role in the transition from fossil fuel to renewable energy. However, the dependency on a moderate to strong aquifer drive being present limits the area where the successful application of this synergy can occur. It is also desirable to have the geothermal production site close to the demand location in order to reduce loss of heat during transport and the costs of a heating grid. Finally,

in order to have an economical supply of heat, a minimum heat demand has to be present, preferably close to the geothermal production site. Godderij et al. (2018) demonstrated that once a heat grid throughout the village of Roden is installed, the demand becomes aligned with economic supply of heat. In theory the above three requirements are met in the study area of this paper. Therefore synergy between gas production and geothermal exploitation with an aligned supply and demand could be applied here. In the Netherlands there are numerous gas fields where a moderate to strong aquifer drive exists, at which the synergy concept of this paper could be applied. However, in some areas, for example Slootdorp, the demand for heat appears to be quite far from the gas production facility, making the economic application of synergy in that area questionable.

Conclusion

The presented simulations and sensitivity analyses on the Roden gas field demonstrate that the placement of a geothermal doublet close to the GWC of a producing gas field may lead to a higher gas recovery factor. The additional revenues can be used to partly finance the geothermal development, thereby reducing the investment risk. The significance of increased gas production predominantly depends on the amount of aquifer support linked to the gas reservoir. Sensitivity analyses indicate that a limited aquifer drive causes the gas- and geothermal production to interfere with one another, resulting in reduced benefits for both the gas recovery and geothermal exploitation. The Roden gas field, which is characterised by a moderate to strong aquifer drive, may achieve significantly higher gas recovery through an optimised gas- and geothermal well configuration. The interplay between gas- and geothermal production is very complex, however, and dependent on location-specific conditions such as the distribution of reservoir parameters and production strategy, including well placement. Performing thorough simulations is therefore key to maximising the benefits.

Although installation of a geothermal doublet in an early phase of gas production delivers the best results, it may still be beneficial to consider installation at a later stage when water breakthrough is emerging or the wells are closed in after full water breakthrough. Synergy with geothermal exploitation may therefore be key to an economic redevelopment of gas fields nearing the end of field life as well as to opening geothermal plays in areas where the initial investment risks are currently blocking developments.

The additional profits obtained from increased gas production due to synergy between natural gas production and geothermal development can be used as an early repayment of the investment costs of the geothermal project, thereby lowering the financial risks.

References

Aramburo Velez, D.A., 2017. Synergy between geothermal and stranded oil fields to add value to geothermal projects. MSc Thesis Report. TU Delft (Delft). Available at https://repository.tudelft.nl/islandora/object/uuid:54e04066-3074-45af-8f1c-d5f5051b9151/datastream/OBJ/download.

Breunese, J., Mijnlieff, H. & Lutgert, J., 2005. The life cycle of the Netherlands' natural gas exploration: 40 years after Groningen, where are we now? In: Doré, A.G. & Vining, B.A. (eds): Petroleum geology: north-west Europe and global perspectives. 6th Petroleum Geology Conference, Geological Society (London): 69–75. Conference proceedings.

Carr, N.L., Kobayashi, R. & Burrows, D.B., 1954. Viscosity of hydrocarbon gases under pressure. Transactions of the American Institute of Metallurgical Engineers 201: 264–272.

Daarnhouwer, M., 2013. Assessing the potential of depleted gasfields for geothermal energy. BSc Thesis Report TA 3009-10, TU Delft. Available at https://repository.tudelft.nl/islandora/object/uuid:a07d9375-82f9-4d22-a562-3352a14f9e27/datastream/OBJ/download.

DAGO (Dutch Association of Geothermal Operators), Stichting Platform Geothermie, Stichting Warmtenetwerk & EBN (Energie Beheer Nederland), 2018. Masterplan Aardwarmte in Nederland. Een brede basis voor een duurzame warmtevoorziening. Available at www.ebn.nl/wp-content/uploads/2018/05/20180529-Masterplan-Aardwarmte-in-Nederland.pdf.

Davis, A.P. & Michaelides, E.E., 2009. Geothermal power production from abandoned oil wells. Energy 34(7): 866–872.

Franco, A. & Vaccaro, M., 2013. Numerical simulation of geothermal reservoirs for the sustainable design of energy plants: a review. Renewable and Sustainable Energy Reviews 30: 987–1002.

Geluk, M.C., 2007. Permian. In: Wong, T.E., Batjes, D.A.J. & De Jager, J. (eds): Geology of the Netherlands. Royal Netherlands Academy of Arts and Sciences (Amsterdam): 63–83.

Geluk, M.C. & De Jager, J., 2012. The development of the oil and gas industry. In: Floor, O.(coord. ed.): Dutch earth sciences – development and impact. KNGMG (The Hague): 208–222.

Godderij, R., Hofman, H., Heusschen, J. & Herber, M.A., 2018. Economic re-use viability of a partially depleted gas field as geothermal doublet. In: AAPG Geothermal Cross-Over Technologies Workshop, 17–18 April 2018, Utrecht, the Netherlands. American Association of Petroleum Geologists (Tulsa, OK).

Honoré, A., 2017. The Dutch gas market: trials, tribulations and trends. Available at www.oxfordenergy.org/wpcms/wp-content/uploads/2017/05/The-Dutch-Gas-Market-trials-tribulations-and-trends-NG-118.pdf.

Juez-Larré, J., Remmelts, G., Breunese, J.N., Van Gessel, S.F. & Leeuwenburgh, O., 2016. Using underground gas storage to replace swing capacity of the giant natural gas field of Groningen in the Netherlands: a reservoir performance feasibility study. Journal of Petroleum Science and Engineering 145: 34–53.

Kramers, L., Van Wees, J.D.A.M., Pluymaekers, M.P.D., Kronimus, A. & Boxem, T., 2012. Direct heat resource assessment and subsurface information systems for geothermal aquifers; the Dutch perspective. Netherlands Journal of Geosciences 91(4): 637–649.

Lensink, S.M. & Van der Welle, A.J., 2018. Basisprijzen en basisprijspremies SDE+ 2018. Available at www.ecn.nl/publicaties/PdfFetch.aspx?nr=ECN-N–17-026.

Lensink, S.M., Cleijne, J.W., Beurskens, L.W.M., Uslu, A., Cremers, M., Lemmes, J., Mast, E., Schulze, P. & Mijnlieff, H., 2018. Eindadvies basisbedragen SDE+. Available at https://www.ecn.nl/publicaties/PdfFetch.aspx?nr=ECN-E–17-048.

Lukawski, M.Z., Anderson, B.J., Agustine, C., Capuano Jr, L.E., Beckers, K.F. & Livesay, B., 2014. Cost analysis of oil, gas and geothermal well drilling. Journal of Petroleum Science Engineering 118: 1–14.

MEA (Ministry of Economic Affairs and Climate Policy), 2016. Energieagenda. Naar een CO2-arme energievoorziening. Available at www.rijksoverheid.nl/binaries/rijksoverheid/documenten/rapporten/2016/12/07/ea/Energieagenda-2016.pdf.

MEA (Ministry of Economic Affairs and Climate Policy), 2018. Natural resources and geothermal energy in the Netherlands 2017. Available at www.nlog.nl/sites/default/files/yearbook%202017-%20englishversion.pdf.

NAM (Nederlandse Aardolie Maatschappij), 2003. Winningsplan Westerveld. Available atwww.dinodata.nl/deliverables/sync/NLOG_FieldAsset_4111_20070706-3-10-Pub_Public_Winningsplan_Westerveld.pdf.

NAM (Nederlandse Aardolie Maatschappij), 2005. Top Rotliegend depth contour map – Roden. Available at www.dinodata.nl/deliverables/sync/NLOG_FieldAsset_1700_ROD_RO.pdf.

Newman, H.H., 1973. Pore-volume compressibility of consolidated, friable, and unconsolidated reservoir rocks under hydrostatic loading. Journal of Petroleum Technology **25**(2): 129–134.

Peters, E., Van Gessel, S.F. & Jedari Eyvazi, F., 2014. An example of synergy between hydrocarbon and geothermal energy production in the Netherlands. *In*: 76th EAGE Conference & Exhibition, June 2014, Amsterdam, the Netherlands. European Association of Geoscientists and Engineers (Amsterdam).

Pluymaekers, M.P.D., Kramers, L., Van Wees, J.D.A.M., Kronimus, A., Nelskamp, S., Boxem, T. & Bonté, D., 2012. Reservoir characterization of aquifers for direct heat production: methodology and screening of the potential reservoirs for the Netherlands. Netherlands Journal of Geosciences **91**(4): 621–636.

RGD (Rijks Geologische Dienst), 1983. Inventarisatie van de Upper Rotliegend Group (Slochteren Sandstone Formation) in Nederland t.b.v. de winning van aardwarmte. Report no. 83DS05EX. Rijks Geologische Dienst (Haarlem).

RGD, 1987. Diepe geothermie in Nederland. Nadere reservoirkarakterisering en technische- en economische aspecten van hergebruik van verlaten putten. Report no. 87KAR08. Rijks Geologische Dienst (Haarlem).

Rijkers, R. & Van Doorn, T.H.M., 1997. Atlas of geothermal resources in the European Community, the Netherlands. Report no. 97-24-A. Netherlands Institute of Applied Geoscience TNO (Utrecht).

Rutte, M., Van Haersma Buma, S., Pechtold, A. & Segers, G.J., 2017. Regeerakkoord 'Vertrouwen in de toekomst'. Available at www.kabinets formatie2017.nl/binaries/kabinetsformatie/documenten/publicaties/2017/10/10/regeerakkoord-vertrouwen-in-de-toekomst/Regeerakkoord+2017-2021.pdf.

Savelkous, J., 2016. Vermilion en ECW werken aan energietransitie in productieput. Available at https://energeia.nl/nieuws/40052460/vermilion-en-ecw-werken-aan-energietransitie-in-productieput.

Savelkous, J., 2018. Aardgasproducent Vermilion stapt in geothermie en biogas. Available at https://energeia.nl/energeia-artikel/40071420/aardgasproducent-vermilion-stapt-in-geothermie-en-biogas.

TNO, 2018. Doubletparameters. Available at www.thermogis.nl/doublet parameters#economisch.

TNO-NITG, 2004. Geological atlas of the subsurface of the Netherlands – onshore. Netherlands Institute of Applied Geoscience TNO (Utrecht): 104 pp.

Van Adrichem Boogaert, H.A. and Kouwe, W.F.P., 1997. Stratigraphic nomenclature of the Netherlands: revision and update by RGD and NOGEPA, Section A, General. Mededelingen Rijks Geologische Dienst **50**: 1–40.

Van der Donk, M., 2008. Geothermie bezig met inhaalslag; hoge kosten en risico's grootste obstakel. Available at http://energeia.nl/nieuws/2008/11/11/geothermie-bezig-met-inhaalslag-hoge-kosten-en-risico-s-grootste-obstakel.

Van der Sar, N.M., 2014. Risk assessment 2014. Available at https://zoek.officielebekendmakingen.nl/blg-346093.pdf.

Van Geuns, L., Juez-Larré, J. & De Jong, S., 2017. Van exporteur naar importeur. De verander(en)de rol van aardgas in Nederland. Available at http://publications.tno.nl/publication/34625382/IkMSR6/TNO-2017-exporteur.pdf.

Van Geuns, L. & Van Thienen-Visser, K., 2017. Editorial. Netherlands Journal of Geosciences / Geologie en Mijnbouw **95**(5): s1–s2.

Van Wees, J.D.A.M., Lokhorst, A. & Zoethout, J., 2007. Re-using E&P wells for geothermal energy. *In*: 69th EAGE Conference and Exhibition incorporating SPE EUROPEC 2007, 11–14 June 2007, London, UK. European Association of Geoscientists and Engineers (Amsterdam).

Van Wees, J.D.A.M., Kronimus, A., Van Putten, M., Pluymaekers, M.P.D., Mijnlieff, H., Van Hooff, P., Obdam, A. & Kramers, L., 2012. Geothermal aquifer performance assessment for direct heat production: methodology and application to Rotliegend aquifers. Netherlands Journal of Geosciences **91**(4): 651–665.

Van Wees, J.D.A.M, Kramers, L., Mijnlieff, H., De Jong, S. & Scheffers, B., 2014. Geothermal and hydrocarbon exploration – the double play synergy. In 76th EAGE Conference and Exhibition, June 2014, Amsterdam, the Netherlands. European Association of Geoscientists and Engineers (Amsterdam).

Veldkamp, J.G., Van Wees, J.D.A.M., Brunner, L.G., De Jong, A.P.A.M., Heijnen, L.J. & Van Langen, C., 2018. Play-based portfoliobenadering, eerste inzicht in zes voordelen voor veilig en verantwoord, kosteneffectief versnellen van geothermie. Available at www.ebn.nl/wp-content/uploads/2018/06/TNO-EBN-rapport-Play-based-portfoliobenadering-geothermie-30-mei-2018-2.pdf.

Wiebes, E., 2018. Ontwerp-instemmingsbesluit Groningen gasveld 2018–2019. Available atwww.rijksoverheid.nl/binaries/rijksoverheid/documenten/besluiten/2018/08/24/ontwerp-instemmingsbesluit-gaswinning-groning enveld-2018-2019/ontwerp-instemmingsbesluit-gaswinning-groningen veld-2018-2019.pdf.

Wiebes, E., 2019. Gaswinningsniveau Groningen in 2019–2020. Available at www.rijksoverheid.nl/binaries/rijksoverheid/documenten/kamerstukken/2019/09/10/kamerbrief—gaswinningsniveau-groningen-in-2019-2020/Kamer brief+-+Gaswinningsniveau+Groningen+in+2019-2020.pdf.

Ziabakhsh-Ganji, Z., Nick, H., Donselaar, M.E. & Bruhn, D.F., 2018. Synergy potential for oil and geothermal energy exploitation. Applied Energy **212**: 1433–1447.

Appendix

Table A1. Simulated cumulative gas production (in BCM) by ROD-102 in January 2017 using the reference model. Values in brackets give relative increase in regard to the base case cumulative gas production. Geothermal producer distance is relative to the GWC; geothermal injector distance is relative to the geothermal producer. Q indicates geothermal flow rate in Sm^3 h^{-1}. Underlined values indicate co-production of free gas in geothermal production well

Base case	Injector = 1000 m				Injector = 1500 m				Injector = 2000 m			
4.68	$Q = 100$	$Q = 150$	$Q = 200$	$Q = 250$	$Q = 100$	$Q = 150$	$Q = 200$	$Q = 250$	$Q = 100$	$Q = 150$	$Q = 200$	$Q = 250$
Producer = 250 m	4.97 (6.2)	5.16 (10.3)	5.26 (12.4)	5.35 (14.3)	5.06 (8.1)	5.16 (10.3)	<u>5.35</u> <u>(14.3)</u>	<u>5.44</u> <u>(16.2)</u>	5.16 (10.3)	5.26 (12.4)	<u>5.44</u> <u>(16.2)</u>	<u>5.55</u> <u>(18.6)</u>
Producer = 500 m	4.87 (4.1)	5.06 (8.1)	5.16 (10.3)	5.21 (11.3)	4.97 (6.2)	5.07 (8.3)	5.16 (10.3)	5.35 (14.3)	4.97 (6.2)	5.16 (10.3)	5.26 (12.4)	5.35 (14.3)
Producer = 750 m	4.87 (4.1)	4.97 (6.2)	5.07 (8.3)	5.07 (8.3)	4.87 (4.1)	4.97 (6.2)	5.07 (8.3)	5.16 (10.3)	4.87 (4.1)	4.97 (6.2)	5.07 (8.3)	5.16 (10.3)

Table A2. Simulated cumulative gas production (in BCM) by ROD-102 in January 2017 for the sensitivity analyses on increased gas production rate, permeability and aquifer. Values in brackets give relative increase in regard to the base case cumulative gas production for the specific scenario. Geothermal producer distance is relative to the GWC; geothermal injector distance is relative to the geothermal producer. Q indicates geothermal flow rate in Sm^3 h^{-1}. Underlined values indicate co-production of free gas in geothermal production well

		Injector = 1500 m								Injector = 2000 m							
		$Q = 100$		$Q = 150$		$Q = 200$		$Q = 250$		$Q = 100$		$Q = 150$		$Q = 200$		$Q = 250$	
$Q_g = 1{,}200{,}000\ Sm^3\ d^{-1}$	**Producer = 250 m**	4.60	(7.5)	4.82	(12.6)	4.93	(15.2)	<u>5.03</u>	<u>(17.5)</u>	4.71	(10.1)	4.82	(12.6)	4.93	(15.2)	<u>5.14</u>	<u>(20.1)</u>
Base case = 4.28 BCM	**Producer = 500 m**	4.60	(7.5)	4.71	(10.1)	4.82	(12.6)	4.93	(15.2)	4.60	(7.5)	4.71	(10.5)	4.82	(12.6)	4.92	(15.0)
Permeability doubled	**Producer = 250 m**	5.17	(6.2)	5.26	(8.0)	5.36	(10.1)	5.46	(12.1)	5.17	(6.2)	5.26	(8.0)	5.36	(10.1)	<u>5.45</u>	<u>(11.9)</u>
Base case = 4.87 BCM	**Producer = 500 m**	5.07	(4.1)	5.17	(6.2)	5.26	(8.0)	5.35	(9.9)	5.07	(4.1)	5.17	(6.2)	5.26	(8.0)	5.36	(10.1)
Permeability trend	**Producer = 250 m**	5.16	(8.0)	5.35	(11.9)	<u>5.50</u>	<u>(15.1)</u>	<u>5.62</u>	<u>(17.6)</u>	5.16	(8.0)	5.44	(13.8)	<u>5.55</u>	<u>(16.1)</u>	<u>5.69</u>	<u>(19.0)</u>
Base case = 4.78 BCM	**Producer = 500 m**	5.07	(6.1)	5.26	(10.0)	5.35	(11.9)	5.45	(14.0)	5.07	(6.1)	5.26	(10.0)	5.45	(14.0)	5.55	(16.1)
Permeability trend inversed	**Producer = 250 m**	4.66	(8.6)	4.84	(12.8)	<u>5.02</u>	<u>(17.0)</u>	<u>5.28</u>	<u>(23.1)</u>	4.66	(8.6)	4.93	(14.9)	<u>5.09</u>	<u>(18.7)</u>	<u>5.27</u>	<u>(22.8)</u>
Base case = 4.29 BCM	**Producer = 500 m**	4.57	(6.5)	4.66	(8.6)	4.84	(12.82)	4.94	(15.2)	4.57	(6.5)	4.75	(10.7)	4.85	(13.1)	5.01	(16.8)
Limited aquifer	**Producer = 250 m**	<u>3.95</u>	<u>(7.1)</u>	<u>3.98</u>	<u>(7.9)</u>	<u>3.98</u>	<u>(7.9)</u>	<u>3.99</u>	<u>(8.1)</u>	<u>3.95</u>	<u>(7.1)</u>	<u>4.01</u>	<u>(8.7)</u>	<u>4.01</u>	<u>(8.7)</u>	<u>4.02</u>	<u>(8.9)</u>
Base case = 3.69 BCM	**Producer = 500 m**	3.93	(6.5)	3.93	(6.5)	3.93	(6.5)	3.94	(6.8)	3.93	(6.5)	3.97	(7.6)	3.95	(7.1)	3.97	(7.6)
Strong aquifer	**Producer = 250 m**	3.98	(7.6)	4.17	(12.7)	4.25	(14.9)	<u>4.38</u>	<u>(18.4)</u>	4.04	(9.2)	4.17	(12.7)	4.32	(16.8)	<u>4.46</u>	<u>(20.6)</u>
Base case = 3.70 BCM	**Producer = 500 m**	3.97	(7.3)	4.04	(9.2)	4.17	(12.7)	4.25	(14.9)	3.98	(7.6)	4.09	(10.5)	4.17	(12.7)	4.32	(16.8)

Table A3. Simulated cumulative gas production (in BCM) by ROD-102 in January 2017 for the sensitivity analyses on timing. TGP = total gas production in BCM; percentage indicates relative increase in regard to the total gas production of the reference model

Scenario	TGP	%
Reference model	4.68	0
Start gas production	5.35	14.3
Halfway before water breakthrough	5.26	12.4
Start water breakthrough	5.07	8.3
Restart gas production 4 years	5.08	8.6
Restart gas production 10 years	5.26	12.4